LASER & PHOTONICS REVIEWS
www.lpr-journal.org

Recent Progress in Dynamically Modulating Lasing Mode Based on External Physical Fields

Junfeng Lu, Yiyao Peng, Wenda Ma, Zheng Yang, Fangtao Li, Chunxiang Xu,* and Caofeng Pan**

The research and development of wavelength-tunable lasers has always attracted much attention due to their huge potential applications in the fields of biomedicine, spectroscopy, information science, and integrated optics. Semiconductor materials with asymmetric center structures, such as ZnO, GaN, CdS, and perovskite, exhibit both piezoelectric and piezoresistive effects, which provide a feasible path for the realization of lasing mode selective output and dynamic modulation. In this review, the dynamic regulation of lasing mode output is obtained in different semiconductor optical cavity in succeed, and realized the single-mode laser by utilizing the synergistic effect of piezoelectricity and piezoresistivity. In addition, the application of this modulated method in the field of nonlinear optics and strain sensing is also further explored and expanded. This series of research results fully proves that this modulation mechanism is not only suitable for the dynamic regulation of the resonant frequency of cavity mode in different material systems, but also provides an effective strategy for the development of a new type of non-contact, high-precision strain sensors by taking advantage of the ultra-narrow pulse width lasing mode-shift.

1. Introduction

Since Theodore Mainman invented the first ruby laser in 1960s,[1] it has achieved important applications in military defense, biomedicine, information communications, industrial manufacturing, and other fields,[2–13] as well as promoting the progress of almost the entire human civilization and driving the development of fundamental research in every field after decades of exploration. As one of the most important branches, semiconductor lasers[14–19] use a mirror surface formed by the cleavage plane of a semiconductor crystal as a resonant cavity to amplify light oscillations and feedback, as well as radiate the laser. The output laser possesses the advantages of a small size, long life, and high efficiency, which is also compatible with existing integrated circuits and easy to realize optoelectronic integration. It has become a hot research direction in the international academic community.

Compared with traditional fixed-frequency lasers, designing and constructing mode-tunable lasers is one of the most important research tasks and an effective way to expand the scope of laser applications. Many efforts in the realization of resonant wavelength tunable lasers have been made through different methods, including energy band engineering of semiconductors,[20–24] self-absorption effect,[25–28] and Burstein–Moss (BM) effect with the participation of surface plasmons.[29–31] In particular, obtaining single-mode laser output and enabling dynamic and sustainable modulation of its

J. Lu
College of Science
Nanjing University of Aeronautics and Astronautics
Nanjing 211106, P. R. China
E-mail: lujunfeng@nuaa.edu.cn

J. Lu
Key Laboratory of Aerospace Information Materials and Physics (NUAA)
MIIT
Nanjing 211106, P. R. China

C. Pan
Institute of Atomic Manufacturing
Beihang University
Beijing 100191, P. R. China
E-mail: pancaofeng@buaa.edu.cn

Y. Peng, W. Ma, Z. Yang
Beijing Institute of Nanoenergy and Nanosystems
Chinese Academy of Sciences
Beijing 101400, P. R. China

C. Xu
School of Electronic Science & Engineering
Southeast University
Nanjing 211189, P. R. China
E-mail: xcxseu@seu.edu.cn

F. Li
School of Physics and Electronic Engineering
Xinyang Normal University
Xinyang 464000, PR China

The ORCID identification number(s) for the author(s) of this article can be found under https://doi.org/10.1002/lpor.202501881

DOI: 10.1002/lpor.202501881

output frequency has always been the goal pursued by scientific researchers, which can avoid the instability and pulse broadening caused by mode competition and group-velocity dispersion in multiple-frequency lasers. At present, the approaches to achieve single-mode operation have been widely reported, such as small-sized optical cavities,[32–34] DBR (distributed Bragg reflector)/DFB (distributed feedback) technology,[35–38] Vernier effect,[39–42] parity-time symmetry breaking,[43–46] pumping optical field modulation,[47,48] etc. However, these modulation methods are not reversible and highly rely on pre-designed cavity configurations and complex micromachining technologies, therefore, an effective research solution is still lacking to achieve dynamic and sustainable lasing mode regulation. In particular, obtaining a continuously adjustable single-mode laser output is rarely reported.

As the active cavity, semiconductor materials, such as ZnO, GaN, CdS, and perovskite, also have special piezoelectric properties[49–54] due to their noncentral symmetric structure. The modulation of the energy band at the interface by the piezoelectric polarization charge as a "gate" generated by the external mechanical strain is used to control the carrier transport process, which provides a new thinking and approach for applications in human-computer interaction,[55–61] micro/nano electromechanical systems,[62–68] sensing[69–81] and self-power systems.[82–88] On the other hand, the external force will cause the positive and negative charge centers to deviate, forming a dipole moment. This will result in the ion polarization inside the crystal, leading to the dielectric constant (refractive index) of the medium to change. And combined with the synergistic effect of the piezoresistivity, it is expected to achieve a dynamic, continuously adjustable lasing mode output, and obtain a single-mode lasing output in needless of pre-designed microcavity configuration and complex micromachining processes.

In this review, we look into the recent progress of dynamically modulating lasing mode output. The fundamental physics of the mode selection mechanism in two kinds of resonant cavities and the regulation mechanism are clarified. And some milestone advances in dynamic regulation of lasing mode for different semiconductor materials systems from multi-mode output to single-mode design are systematically reviewed, and extending to the modulation of nonlinear optical signals. Furthermore, we are finally looking forward to the application of lasing mode shift in the construction of high-precision, non-contact strain sensors based on color perception, and explored the possibility of further application in high-resolution pressure imaging.

2. Regulation Mechanism

2.1. Piezoelectric Effect

Piezoelectric effect refers to the physical phenomenon that when certain media, such as some semiconductors of ZnO, GaN, CdS, and perovskite is subjected to external strain in a specific direction, positive and negative charge centers are separated to form an electric dipole moment, causing the internal polarization, then resulting in the accumulation of positive and negative charges on two opposing surfaces. In 2006, Z. L. Wang et al.[89] from Georgia Institute of Technology discovered the piezoelectric effect in ZnO nanowires with asymmetric center structure and constructed the first piezoelectric nanogenerator in the world. Since then, the application of the piezoelectric effect in the field of optoelectronics has received widespread attention and achieved vigorous development.[90–98] Then, after several years of development, two original fields of piezotronics and piezophototronics were formed and proposed by Wang and co-workers in 2007 and 2010, respectively, based on three-field coupling between semiconductors, photoexcitation, and piezoelectricity.[99–105] In addition, as early as 1969, Vedam et al.[106] found in experiments that the dielectric polarization caused by external mechanical perturbations has a greater effect on its own refractive index than the change in the number of dispersion centers per unit volume in hexagonal crystals. Moreover, this adjustment of the refractive index in the elastic strain range is dynamic, sustainable, and reversible, which does not require any complicated micromachining process conditions. It provides a feasible approach for the dynamic modulation of lasing mode under strain.

2.2. Piezoresistive Effect

Piezoresistive effect refers to the physical phenomenon that when a certain semiconductor is subjected to a stress in a certain direction, its energy band will change to form the bandgap recombination, leading to a change in resistivity. It was first discovered by C. S. Smith in the resistivity and stress variation characteristics test of silicon and germanium in 1954.[107] Moreover, it exhibits anisotropic characteristics, that is, when the strain is applied in different crystal directions, the resistivity changes will be different. In addition, the band gap recombination caused by the piezoresistive effect can not only cause a change in electrical properties, but also a change in optical properties, which will lead to a shift of the spontaneous emission peak in a direct band gap semiconductor. As in a large number of previous reports, people have implemented dynamic regulation of PL (photoluminescence) peaks by applying external mechanical strains on wurtzite ZnO, GaN, and CdS.[108–113] Simultaneously, as an active cavity, this excitonic energy-related regulation is just an effective way to modulate the optical gain region, and provides a feasible strategy for subsequent selective lasing mode output. Combined with the above-mentioned piezoelectric effect, it is expected that single-mode laser output can be achieved in a micron-sized optical resonator by using the relative shift between the optical gain region and the resonant mode frequency.

2.3. Mode Selection

2.3.1. Typical F-P Cavity

Figure 1 shows the basic composition of a typical FP (Fabry-Pérot) laser resonator,[114] containing three necessary conditions of a pumping source, a gain medium, and a cavity for laser generation. At the steady-state oscillation condition, the obtained optical gain and phase shift for a light-wave with a frequency of ω through a complete feedback loop must satisfy the following equation

$$\frac{\varepsilon_1}{\varepsilon_2} \equiv r_1 r_2 \exp\left(2\alpha_m L_m - \frac{i2\omega L}{c}\right) = 1 \quad (1)$$

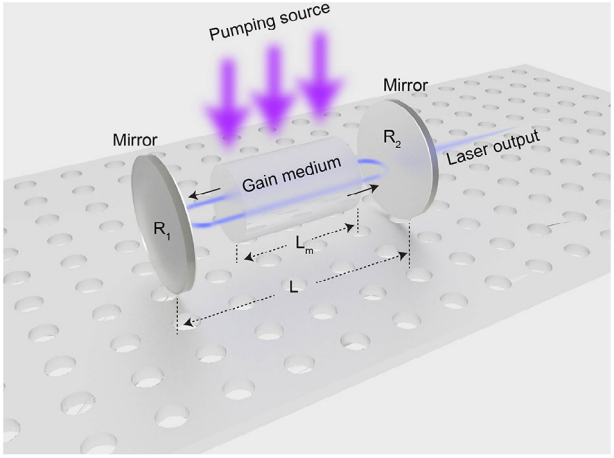

Figure 1. Elements of a typical F-P cavity. Three essential conditions for generating a laser: a gain medium which can supply stimulated emission, a resonance cavity to supply the feedback and oscillation and a pumping source to achieve population inversion.

where the ϵ_1 and ϵ_2 represent the electromagnetic fields before and after the light-wave passes through the gain medium, r_1 and r_2 are the reflection coefficients of the light wave-amplitude at the two end mirrors; the first exponent term $\exp(2\alpha_m L_m)$ represents the round trip light amplification through the laser gain medium of length L_m, and the second exponent term $\exp(-i2\omega L/c)$ is the round trip phase shift around the laser cavity of Length L. It indicates that the light wave (ϵ) propagates a round trip inside the cavity, and get reflected twice at the cavity boundaries. After that, it must equal to itself to achieve lasing state. The former defines the amplification conditions, which determine the minimum population inversion required to achieve oscillation in the gain medium. It can be expressed as:

$$r_1 r_2 \exp\left(2\alpha_m L_m\right) = 1 \text{ or } \alpha_m = \frac{1}{4L_m}\ln\left(\frac{1}{R_1 R_2}\right) \tag{2}$$

where $R_1 = |r_1|^2$ and $R_2 = |r_2|^2$ are the reflectivities of the two end mirrors. It reflects that the gain or loss of the cavity is inversely proportional to the gain length, which means that, a smaller gain is always accompanied by a higher loss. The latter defines the size of the laser cavity, which determines that the round-trip phase-shift in the laser cavity must be an integer multiple of 2π, or the length of the round-trip loop is an integer multiple of wavelengths at the oscillation frequency. It can be expressed by the following equation.

$$\exp\left(-\frac{i2\omega L}{c}\right) = \exp\left(-iN2\pi\right) or - i\frac{2n_{eff}L2\pi}{\lambda} = -iN2\pi, N = 1, 2, 3, \ldots \tag{3}$$

where n_{eff} is the effective refractive index of the cavity, λ is wavelength, and N is integer. It reflects that the shortest cavity length required to generate the lasing output of the fundamental longitudinal mode, which is equals to $\lambda/2n_{eff}$. When the round-trip phase-shift condition of the light-wave oscillation is satisfied in a selected resonator, a set of discrete optical longitudinal modes can be selected and amplified.

2.3.2. The Plane Wave Model for WGM Cavity

Similar to a linear F-P cavity, the resonance condition for the conventional WG (whispering-gallery) modes can be given by

$$\frac{2\pi R n_{eff}}{\lambda} = N, N = 1, 2, 3, \ldots \tag{4}$$

where R is the radius of the circular or spherical microcavity for the conventional WGM modes. The whispering-gallery hexagonal resonator is regarded as a special case of the ring laser oscillator, where the laser generation must also satisfy the steady-state oscillation condition. **Figure 2**a demonstrates the schematic diagram of the light propagation path (marked with the white arrows) in a hexagonal cavity.[115] The light waves propagate along the six crystal planes of the resonator and are total internally reflected on the inner walls, as shown in the electromagnetic field distribution diagram of Figure 2b. Most of the light field energy is localized in the optical microcavity due to the total reflection at the interface, and only a small part is radiated outward from the six corners (marked with red arrows). To clarify the oscillation mechanism of light in the hexagonal WGM microcavity, Wiersig et al.[116] proposed a plane wave model based on semi-classical quantization theory. According to Fresnel formula, the reflectance of TE (transverse electric) and TM (transverse magnetic) polarized light can be described as follows:

$$\mathrm{r} = \frac{1 - i\alpha}{1 + i\alpha} \tag{5}$$

with

$$\alpha = \frac{\beta\sqrt{n^2 sin^2\theta_i - 1}}{cos\theta_i} \tag{6}$$

where θ_i is the angle of incidence, n is the refractive index, β equals to n for TE modes, and equals to $1/n$ for TM modes. Let $\alpha = \tan\theta$, the Fresnel formula can be simplified as,

$$\mathrm{r} = \exp\left(-i2\theta\right) \tag{7}$$

According to the steady-state oscillation conditions, when the light wave propagate along the inner wall of the resonant cavity through a complete feedback loop, the phase shift must meet an integer multiple of 2π, namely,

$$\left[\exp\left(\frac{in2\pi L_p}{\lambda}\right)\right] r^m = 1 \tag{8}$$

where L_p is the length of the propagation path, λ is the resonant wavelength, m is the number of resonant cavity edges. In our case, taking the hexagonal WGM microcavity as an example and only considering TE polarization, we can get $\beta = 1/n$, $m = 6$,

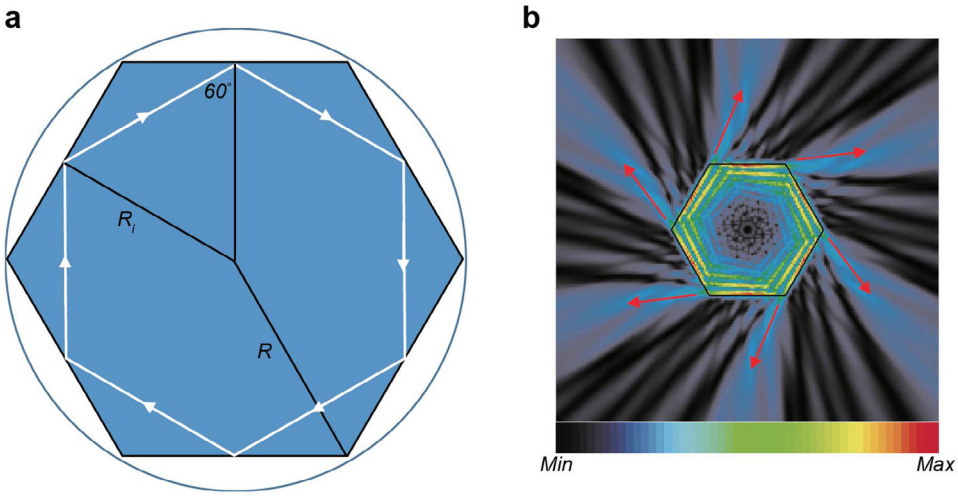

Figure 2. Whispering-gallery oscillation model in a hexagonal cross-section structure. a) A schematic of the light confined in a hexagonal resonator and the propagation path as indicated by the white arrows. Reproduced with permission.[115] Copyright 2004, American Physical Society. b) The simulation of the electromagnetic field distribution in a 2D hexagonal resonator. Reproduced with permission.[116] Copyright 2003, American Physical Society.

$\theta_i = 60°$ and $L_p = 3\sqrt{3}R$. Combined with Equations (7) and (8), it is deduced that

$$n\frac{2\pi}{\lambda}L_p - 12\theta = N2\pi,\ N = 1, 2, 3, \ldots \tag{9}$$

Then,

$$N = \frac{3\sqrt{3}nR}{\lambda} - \frac{6}{\pi}tan^{-1}\left(n\sqrt{3n^2-4}\right) \tag{10}$$

where R is the radius of the hexagonal cavity. Therefore, despite the different resonator structures, the basic principle of mode selection is completely uniform, that is, both of them must meet the round trip phase shift conditions. Similarly, in Equation (8), if we set $m = 4$, $\theta_i = 45°$ and $L_p = 4\sqrt{2}R$. respectively, the resonance condition of the square whispering gallery microcavity[117,118] can also be derived. It can be seen that the output frequencies of the resonant cavity modes are closely related to the refractive index and size of the resonator. This provides a feasible strategy for us to dynamically manipulate the output of the laser mode.

3. Piezoelectric Effect Tuned Lasing Mode

3.1. Mode Regulation in Single ZnO Microcavity

ZnO is a typical non-central symmetric semiconductor material with a special piezoelectric effect.[89] In addition, it has an excitonic binding energy of up to 60 meV and a direct wide bandgap energy of 3.37 eV, making it an excellent candidate for building short-wave optoelectronic devices,[119–122] especially laser devices.[123–125] In recent years, many investigations on optical pumping lasers of ZnO have been reported.[126–131] Combined with the intrinsic physical characteristics of piezoelectricity for wurtzite-structural ZnO, it is expected to achieve dynamic sustainable regulation of its lasing mode.[132,133] The optical path system and measurement setups shown in **Figure 3a** were used for spectral collections and external mechanical strain application. A nanosecond pulsed laser with a wavelength of 355 nm is used as an excitation source to optically pump a high-quality single-crystal ZnO microcavity. Figure 3b shows the optical photographs of the ZnO microcavity under the excited state at different excitation energies. When the pumping power (P_{in}) is below the excitation threshold (P_{th}), the intrinsic photoluminescence of ZnO blue-violet can be observed in the middle panel of dark-field. As $P_{in} > P_{th}$, the dazzling blue-violet light emitted from the edges of hexagonal ZnO microcavity. To reveal the oscillation mode of light waves in an optical microcavity, the plane wave model as mentioned in Section 2.3 has been used to analyze the lasing spectrum with a full width at half maximum (FWHM) of ≈0.3 nm at a pumping power of 15.6 mW shown in the middle panel of Figure 3c. The lasing Q factor can be estimated as ≈1300 according to the equation of $Q = \lambda/\Delta\lambda$. The number of TE modes can be assigned as 71, 70, 69, 68 and 67 with the resonant wavelength of 390.40, 391.58, 392.77, 394.07, and 395.51 nm as shown in the up panel of Figure 3c, which is matched well with the experimental results. When a tensile strain was applied along the *c*-axial direction of ZnO, it can be observed that the resonant wavelength of TE mode significantly shifts toward the long wavelength direction, accompanied by the disappearance of higher-order modes and the appearance of lower-order modes, as shown in Figure 3d. The resonant wavelength of TE_{67} shifts from 395.51 nm to 397.45 nm with the tensile strain increasing from 0% to 0.95%. As the applied tensile strain is 0.51%, the TE_{67} mode line is completely separated, which is almost no overlap area shown in the below panel of Figure 3e. For the NBE (near-band emission), the PL lines almost completely overlap each other under similar tensile strain, as shown in Figure 3h. Therefore, it will greatly improve the resolving capacity of strain detection through the lasing mode-shift due to its narrow FWHM. To clarify the regulation mechanism of lasing mode caused by tensile strain, we estimate the refractive index of each mode under different tensile strains according to the calculation formula of the mode number, accompanied by comprehensive consideration of

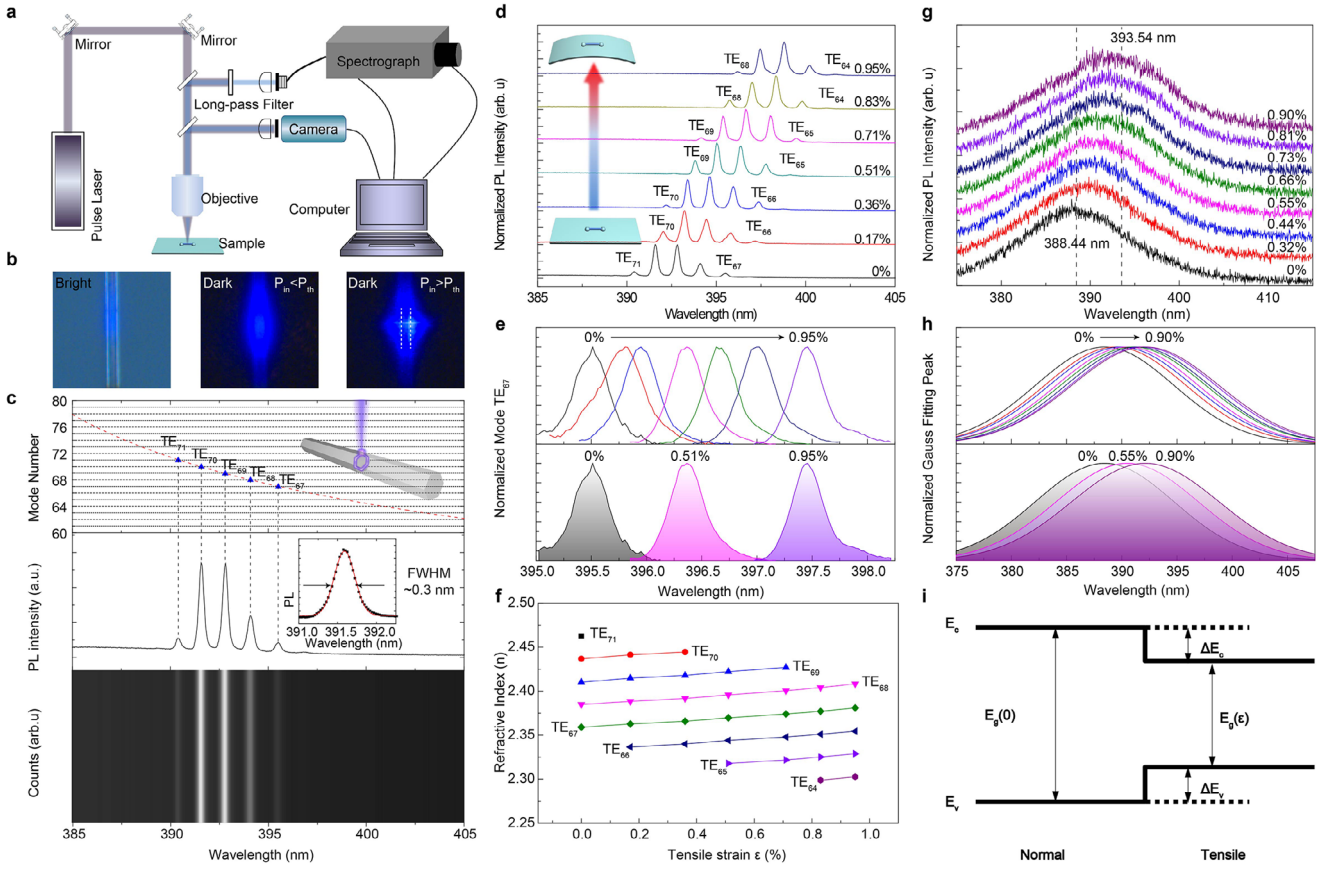

Figure 3. ZnO WGM lasing modulation. a) Optical system; b) Optical images of single ZnO microrod under the excitation of 355 nm nanosecond laser, left panel: bright-field, middle panel: $P_{in}<P_{th}$ (dark-field), right panel: $P_{in}>P_{th}$ (dark-field); c) Calculated TE mode number, lasing spectrum and mapping as the pumping power exceeds the threshold; d) Lasing spectra of the same ZnO microrod under different tensile strains; e) the mode-shift of TE_{67} with the tensile strain changing from 0% to 0.95%; f) the dependence of the calculated refractive index and the tensile strain; g) PL spectra of same ZnO microrod under different tensile strains; h) PL shift with the tensile strain increasing from 0% to 0.90%; i) Schematic diagram of energy band structure under the normal and tensile conditions. Reproduced with permission.[132] Copyright 2018, American Chemical Society.

the cavity size change caused by the Poisson effect, as shown in Figure 3f. It illustrates that the change in refractive index caused by crystal polarization under external mechanical strain (piezoelectric effect) is the dominant factor leading to the redshift of TE mode, because the reduced cavity can only cause the blueshift. In addition, the redshift of NBE emission (optical gain region) caused by the piezoresistive effect provides a strong guarantee for the sustainable regulation and mode selection of the lasing mode. The organic combination of the two provides an important idea for the realization of dynamic, regulated lasing mode and color-resolved strain sensing components. On the other hand, directly manipulating nanoscale samples at the microscale has always been a pursued goal. Compared to traditional micro/nanomanipulation, photothermal-shock tweezers represent a novel approach for achieving spatial dynamic reconfiguration at the micro-scale with advantages of versatility, nanoscale precision, real-time operation, and large external output force. For instance, Zhu et al.[134,135] demonstrated the in situ spatial dynamic reconfiguration of plasmonic nanowire devices and circuits on dry solid substrates through this technique. Simultaneously, they successfully achieved single-mode/multi-mode switching and mode optimization by precisely controlling the relative positions of the photonic cavity (CdSe nanowire) and plasmonic cavity (Au nanowire). This opens new avenues for reconfigurable nanoplasmonic structures with dynamically tunable spatial characteristics.

3.2. Mode Regulation in Single GaN Microrod

Subsequently, we have also achieved dynamic regulation of the shorter-wavelength intrinsic WGM lasing mode in another typical third-generation semiconductor material of GaN.[136] It has broad prospects and application spaces in optoelectronics, high power devices, and high frequency microwave sensors, due to its wide-bandgap semiconductor with wurtzite structure and superior stability. In addition, Therefore, GaN-based strain sensor is fabricated, which senses the stress change via the shift of lasing mode on account of the piezoelectric effect, with lots of advantages including superior color-resolvability, high resolution, noncontact interactions, flexibility, transparency, and a simple construction. According to the linear relationship between the redshift amount of TE_{101} mode photon energy and applied tensile strain, the magnitude of corresponding mechanical

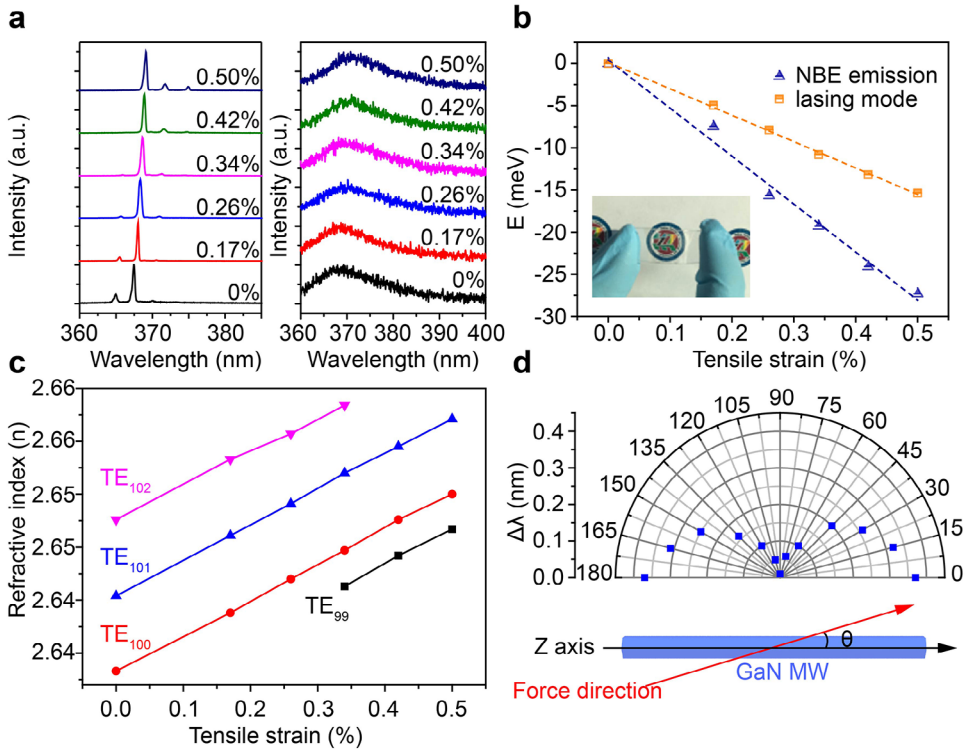

Figure 4. Lasing mode regulation in single GaN microrod. a) Strain-induced the shift of lasing mode and PL spectra. b) The dependence of photon energy on applied tensile strain for PL spectra and lasing mode, respectively. The inset shows the flexible and transparent strain sensor based on GaN microrod. c) The relationship between refractive index and the tensile strain for different TE modes. d) The change of lasing mode as a function of the included angle θ for the same GaN microcavity. Reproduced with permission.[136] Copyright 2019, John Wiley and Sons.

stress can be quantified, as shown in **Figure** 4b. However, the inner mechanism of PL shift and lasing mode shift shown in Figure 4a is entirely different. The former is attributed to the strain-induced energy bandgap variation, so-called piezoresistive effect, while the latter is due to the strain-induced refractive index variation caused by internal piezoelectric polarization of the crystal, namely, piezoelectric effect. Figure 4c demonstrates the dependence of the refractive index for different resonant modes on the external tensile strain, which is estimated through the plane wave model. Compared with strain-induced PL emission shift, the lasing mode variation-based strain sensor has a higher resolution and a superior color-resolvability. Moreover, the angle-dependent lasing spectra have also been investigated, where the angle refers to the included angle of the applied stress direction and *c*-axis directional GaN microrod, as shown in Figure 4d. Furthermore, compared with ZnO, GaN-based strain sensors have wider potential applications due to their excellent stability and commercial conformability. Specifically, the strain sensors fabricated with GaN microwire exhibit a more stable performance at ambient temperature and pressure and have potential applications in extreme environment, including intense radiation, high temperature, strong acidity, and alkalinity situations. Additionally, GaN-based strain sensors possess better commercial and industrial conformability since III-V semiconductors have been widely applied in commercial optoelectronic integrated devices. In brief, it is necessary to fabricate a stable and commercial-conformability GaN-based strain sensor, which could be a significant step in the field of non-contact stress measurement under extreme conditions, long-range strain detection, color tunable pressure mapping, and optical signal modulation.

3.3. The Effect of Crystal Orientation on Mode Regulation in CdS Microbelts

To investigate the effect of crystal orientation on the lasing mode modulation, two crystal orientations of CdS microbelts have been fabricated and used to investigate this mechanism of the modulation under applied tensile strain.[137] As has been reported in the wurtzite CdS structure,[138] the applied strain parallel to the [001] crystal direction will generate the most dipole moment because of the maximum piezoelectric coefficient in this direction, which derives from the more pronounced non-centrosymmetric structure in the [001] orientation. Two morphologies of parallelogram- and ladder-shaped CdS microbelts shown in **Figure** 5b,i were fabricated to explore optical properties, whose growth directions were parallel and perpendicular to the [001] crystal orientation, respectively. As the strain is applied along the growth direction of these two types of CdS microbelts, two force-adding modes can be obtained. When a tensile strain is applied on the parallelogram-shaped CdS microbelts along [001] direction, the red shifts could be found in lasing mode, as shown in Figure 5e. In contrast, as a tensile strain is applied on the growth direction of ladder-shaped

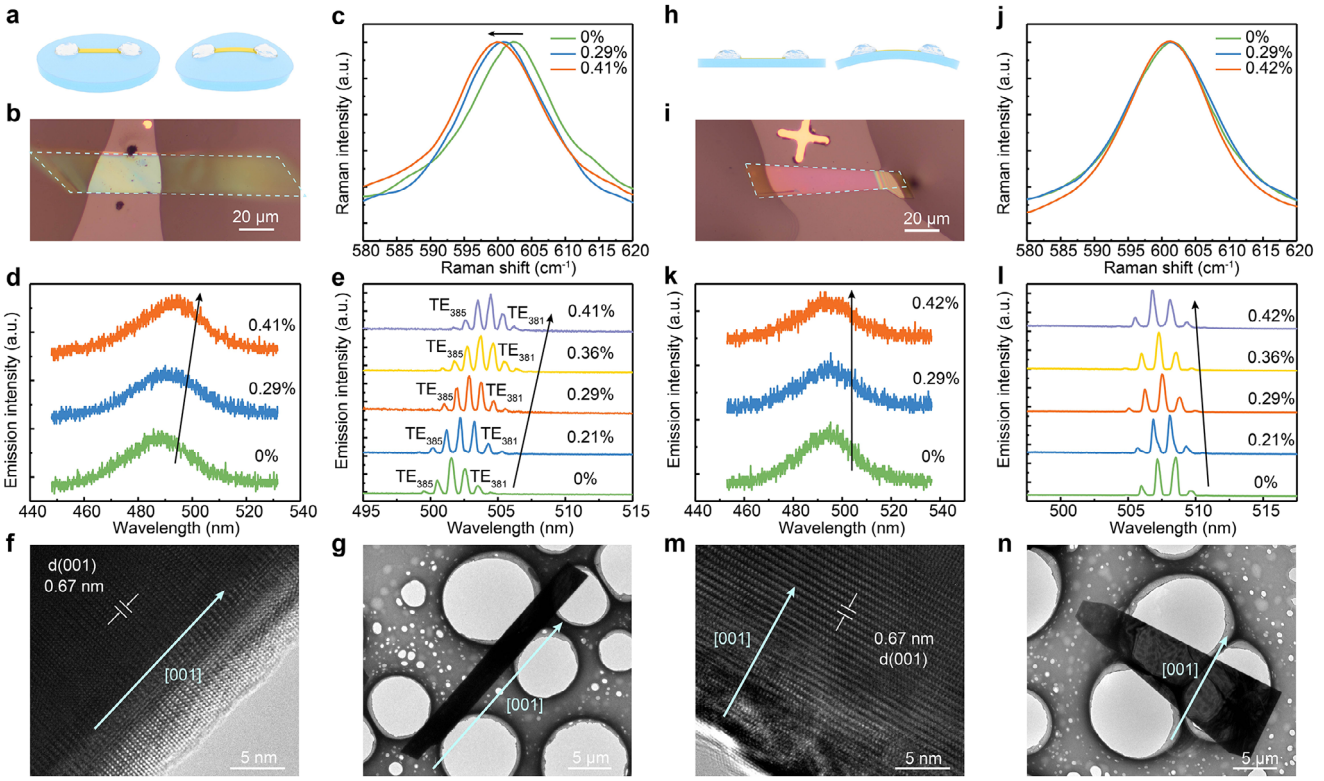

Figure 5. Optical dynamic regulation for CdS microbelts with different lattice orientation. a) Schematic diagram of individual CdS microbelt fixed to the flexible PET substrate under the normal and tensile states. b) Optical image of a parallelogram-shaped CdS microbelt. c) 2-LO peak from the CdS Raman spectra under different tensile strain. Strain-dependent PL d) and lasing e) spectra of CdS microbelt with the TE mode numbers N = 385...381. f) HRTEM image of the parallelogram-shaped CdS microbelt. g) TEM image of individual CdS microbelt with the [001] growth direction. h) Side view of schematic diagram of single CdS microbelt under normal and tensile states. i) Optical image of a ladder-shaped CdS microbelt. j) 2-LO peak from the Raman spectra measured in the ladder-shaped CdS microbelt under different tensile strain. Strain-dependent PL k) and lasing l) spectra of the ladder-shaped CdS microbelt. HRTEM m) and TEM n) image of the ladder-shaped CdS microbelt perpendicular to the [001] growth direction. Reproduced with permission.[137] Copyright 2019, American Chemical Society.

CdS microbelt (perpendicular to [001] direction), the blue shifts shown in Figure 5l appear in the lasing peak. In brief, the strain-induced shifts of the lasing modes resonant wavelength highly depend on the angle between the force and [001] direction of CdS microbelts. The former is attributed to an increase in the refractive index of the optical microresonator caused by the applied tensile strain, while the latter is due to the strain-induced reduction of the cavity size. According to the mode selected formula of a typical F-P cavity $\lambda = \frac{2n_{eff}L}{N}$, the increased effective refractive index (n_{eff}) caused by the piezoelectric polarization effect will lead to the red shifts of lasing mode, while the length of the resonator (L) decreases because of the Poisson effect corresponding to the blue shifts of lasing mode. The value of the red shifts (2.9 nm) under 0.41% strain is almost twice as large as that of the blue shifts (1.6 nm). Summarily, both the refractive index and cavity size tuned by piezoelectric effect and Poisson effect, respectively, play an important role in modulating the lasing mode. In addition, the shifts in PL and Raman emission shown in Figure 5c,d have also been observed when a tensile strain is applied parallel to the [001] direction, where the former indicates the recombination of the NBE band gap, the latter reflects the changes in the frequency of lattice vibration caused by the deformation.[139] In contrast, as the strain is perpendicular to the piezoelectric direction, the peaks of PL and Raman remain unchanged, and only resonator (L) decreases can be deduced by the Poisson effect, which demonstrating that the intrinsic characteristics of the CdS, including the effective refractive index are almost not changed. Indeed, the piezoelectric polarization is able to affect the intrinsic characteristics of the CdS material, such as bond vibration, band gap, and refractive index. In accordance with the shifts of PL emission, Raman spectra, and lasing modes, a concept is provided in this work for designing the innovative pressure sensing, dynamically selecting the resonant mode, tuning the mode-phase, and tunable waveguides. These double modulations of the lasing mode have great significance for the further studies of lasing research.

3.4. Lasing Mode Regulation Based on Thermo-Optic Effect

In addition to the regulation method based on external mechanical strain, the refractive index change induced by the intrinsic thermo-optic effect of microcavities is also a crucial approach for realizing dynamic regulation of laser modes.[140,141] **Figure 6a**

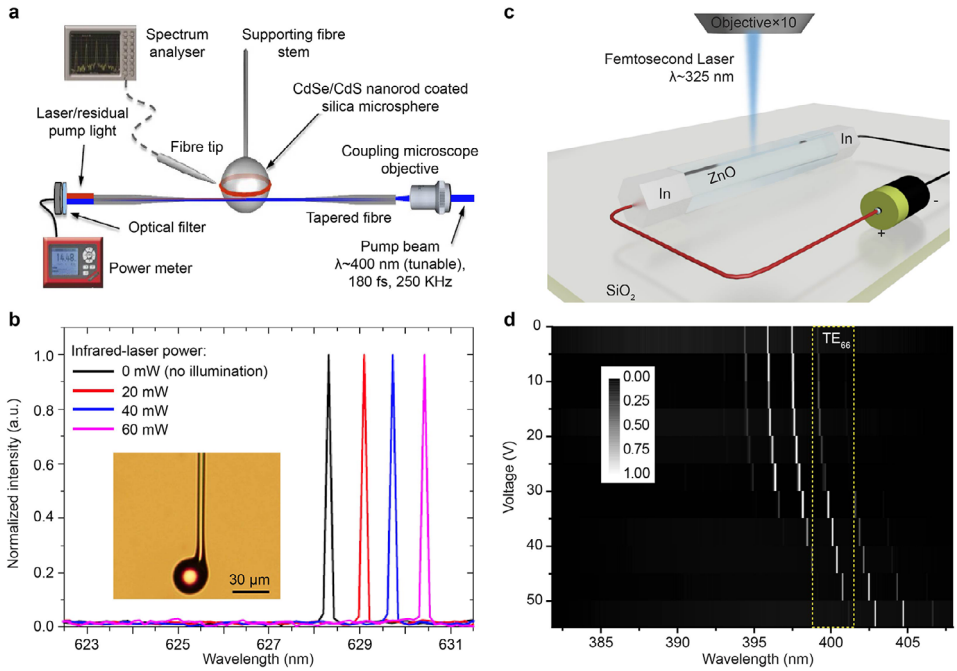

Figure 6. Whispering-gallery mode regulation based on thermo-optic effect. a) Experimental setup for demonstration of lasing in CdSe/CdS colloidal nanorods. b) Tunable laser emission from CdSe/CdS nanorods under different output powers of the infrared-laser. Reproduced with permission.[140] Copyright 2013, The Authors. c) Schematic diagram of electrical injection and the femtosecond pulsed laser excitation (325 nm, 1 kHz, 100 fs). d) 2D images of lasing spectra under different bias voltages. Reproduced with permission.[141] Copyright 2021, AIP Publishing.

presents a schematic diagram of the experimental setup for stimulated emission and detection of a microsphere cavity (see the inset of Figure 6b), where the excitation is performed using a femtosecond laser with a wavelength of 400 nm and a pulse width of 180 fs. This pumping light is evanescently coupled to the microsphere cavity via a tapered fiber with adiabatic transition. Furthermore, a near-infrared laser (with a wavelength of 3.5 μm and a pulse width of 200 fs) is directly focused onto the microsphere cavity using an optical microscope to heat it, thereby achieving dynamic regulation of the lasing wavelength from ≈628.3 to ≈630.4 nm. Various factors contributing to the wavelength shift caused by the thermal effect were systematically investigated, which can be mainly attributed to the change in refractive index.

In comparison, Joule heat generated by electric current is a more straightforward method, as illustrated in Figure 6c. While pumping with a femtosecond laser at a wavelength of 325 nm, a bias voltage is applied to the Ga-doped ZnO microcavity. As the bias voltages gradually increases from 0 to 50 V, a significant red-shift phenomenon occurs in the resonant wavelength of the lasing mode. For the TE_{66} mode, the wavelength changes from 399.26 to 401.26 nm, as shown in Figure 6d. Furthermore, an in-depth analysis was conducted on the relationship between the wavelength variation and the output electrical power, which exhibits a linear correlation. This indicates that the refractive index change induced by Joule heat is the dominant factor for wavelength modulation. Although the regulation method based on the thermo-optic effect is more easy to operate than that based on external mechanical strain, it also has certain drawbacks, such as an increase in the lasing threshold and the broadening of the lasing mode.

4. Single-Mode Realization and Dynamic Regulation by the Piezoelectric and Piezoresistive Synergistic Effect

4.1. Realization and Dynamic Regulation of Single-Mode Lasing Output in Micro-Sized ZnO Cavity

Because of the good monochromaticity and modeless competition, the development of single-mode laser output has drawn much attention from researchers due to its wide application in display, biomedicine, information interaction, and defense. Therefore, various methods of single mode operation have been proposed,[142–145] such as reducing cavity size, distributed Bragg reflection (DBR)/distributed feedback (DFB), Vernier effect, and parity-time symmetry breaking, etc. However, the methods mentioned above impose very stringent requirements on the predesign precision and preparation process of the optical cavity, and meanwhile, cannot meet the requirements of dynamic regulation of the lasing mode output. Therefore, there is an urgent need to develop a new method for continuously and dynamically regulating single-mode lasing output. According to the steady-state oscillation condition of the laser, the fundamental mode oscillation can be satisfied only when the size of the optical microcavity is greater than or equal to 1/2 of the wavelength. Therefore, in theory, single mode lasing-output can be achieved when the cavity is reduced to half the emission wavelength. However, the negative impact of the cavity reduction is a sharp increase in optical loss and laser threshold, which hinders further commercial applications. Recently, we realized the selective output and dynamic regulation of single-mode laser in the relatively small ZnO optical microcavity with a diameter of 1–2 microns by the syner-

gistic effect of piezoelectric polarization effect and piezoresistive effect.[146] For active cavities such as ZnO microrods, the optical gain region has a certain range of wavelengths. Therefore, the mode spacing directly determines the number of the generated TE modes.

Figure 7a shows the SEM (scanning electron microscope) images and electric-field distributions of the fundamental mode in the optical microcavity with different diameters. The simulation results show that the size reduction causes the number of oscillation modes to decrease, which is consistent with the experimental results. Figure 7b shows the lasing and PL spectra of the same ZnO microrod at different strains. The process of multimode to single mode evolution can be observed in the left panel, as the tensile/compressive strains are applied. In addition, it is worth noting that the movement tendency (rate of change) of the PL spectrum is inconsistent with that of the lasing spectrum, as shown in Figure 7d. The yellow dashed line represents the shift of the lasing mode, while the red dashed line represents the PL shift. It can be seen that the variation trend of the envelope of the resonant modes is the same as that of PL, indicating that the optical gain region is closely related to the position of the NBE emission peak. Figure 7c shows the lasing spectra under the strains of −0.96% and 0.94%, respectively. The resonant wavelength can be tuned from 386.06 to 395.36 nm, with a range of 9.3 nm. According to the formula of $SMSR = 10\log(M_1/M_2)$, the side mode suppression ratio (SMSR) in the tensile and compressive states is estimated as 16.4 and 13.2 dB, where M_1 and M_2 represent the intensity of dominant mode and side mode. In order to systematically analyze the mode regulation mechanism, we propose a synergistic action of the piezoelectric polarization effect and the piezoresistive effect, as shown in Figure 7f. In the normal state, two optical longitudinal modes highlighted by violet solid line are selected because they are located in the optical gain amplification region, where gain is greater than loss. As the tensile strain stain is applied, the optical gain region and longitudinal modes move toward the long wave direction together, but the former moves faster than the latter, which leading to the disappearance of the higher-order modes and the formation of single-mode lasing output. It illustrates that except for the influence of the refractive index change caused by the piezoelectric polarization effect shown in Figure 7e on the sustainable regulation of lasing mode, the energy band structure recombination caused by the piezoresistive effect plays a crucial role in the movement of the gain region and mode selection. Figure 7g demonstrates the position of dominant mode and optical dark-field photograph for the same ZnO microcavity under three states of compression, normal and tension. As the external strain changes from compression to stretching, the transformation in laser color can be distinctly observed, laying a solid foundation for further advancement of stress sensor construction with color resolution as the signal source.

4.2. Piezoelectric-Effect-Induced Dynamic Modulation of Single-Mode-Lasing in Monocrystalline $CsPbBr_3$ Perovskite Cavity

Due to their superior optoelectronic characteristics, such as a high absorption coefficient, a long carrier lifetime, a low trap density, a low nonradiative recombination rate, and efficient photoluminescence,[147–150] Lead halide perovskites have become an ideal material for laser applications. As ABX_3-type materials, they possess intrinsic piezoelectric and ferroelectric properties.[151,152] Based on their piezoelectric effect, lead halide perovskites have been used to fabricate nanogenerators and other devices in previous reports.[153–155] And also, the change of dielectric constant (refractive index) caused by the piezoelectric polarization in lead halide perovskites can realize the effective modulation of lasing modes.

Recently, we demonstrated the controllable growth of well-aligned monocrystalline $CsPbBr_3$ microwire arrays.[156] These microwires could serve as high-quality WGM microcavities with high quality factors, low thresholds, and long stability. Moreover, the continuously modulated lasing modes is realized by applying the strains. As shown in **Figure** 8a, the aligned $CsPbBr_3$ MW arrays exhibit uniform sizes, smooth surfaces, and rectangular cross-sections with sharp edges, indicating the monocrystalline nature. The HRTEM(high-resolution transmission electron microscopy) and corresponding SAED (selected area electron diffractio) pattern shown in Figure 8b verify that the MW belongs to the orthorhombic crystal structure with the [010] zone axis. Therefore, the growth of MWs is along the [010] orientation. The different $CsPbBr_3$ MWs were then transferred and fixed onto circular PEN (polyethylene naphthalate) substrates for further lasing tests with a femtosecond laser of 355 nm serving as the uniform pump source. The External mechanical strain applied by manual stage is introduced to realize the dynamical modulation of lasing modes. Two distinct lasing modes of TE_{43} and TE_{42} can be observed with no strain applied when the pumping power exceeds the lasing threshold. From the left panel of Figure 8d, with the increase of compressive strain, a slight blue-shift in PL emissions occurs. In contrast, the PL emissions move in long wave direction with the increase of tensile strain. The change trend of lasing mode is similar to the PL peak under the externally applied strain. In order to intuitively feel the deformation of the perovskite single crystal, a schematic diagram showing the polarization is given in Figure 8c. $CsPbBr_3$ consists of a framework of corner-sharing $PbBr_6$ octahedra and Cs cations in the dodecahedral A sites. It will lead to distortion of the lattice when the strain is applied along the [010] direction, and resulting in the piezoelectric potential. Therefore, piezoelectric polarization will occur in $CsPbBr_3$ with applied strain. If the change of cavity size caused by the Poisson effect is considered, a slight blue-shift of lasing modes should be obtained under the applied tensile strain along the [010] direction. Conversely, compressive strain will cause cavity size to increase, and leading to a redshift of the lasing mode, which is inconsistent with our experimental results. Therefore, the changing of refractive index induced by the piezoelectric polarization effect is the dominant factor that causes the lasing mode to move (Figure 8g,h). This work not only provides a new method for preparing high-quality $CsPbBr_3$ arrays, but also proposes a new strategy for dynamically modulating the lasing modes of lead halide perovskites based on the piezoelectric effect.

5. Dynamic Regulation of Two-Photon-Pumped WGM Lasing

Nonlinear optics is an important branch of modern optics, and its rise is closely related to the development of lasers. Since

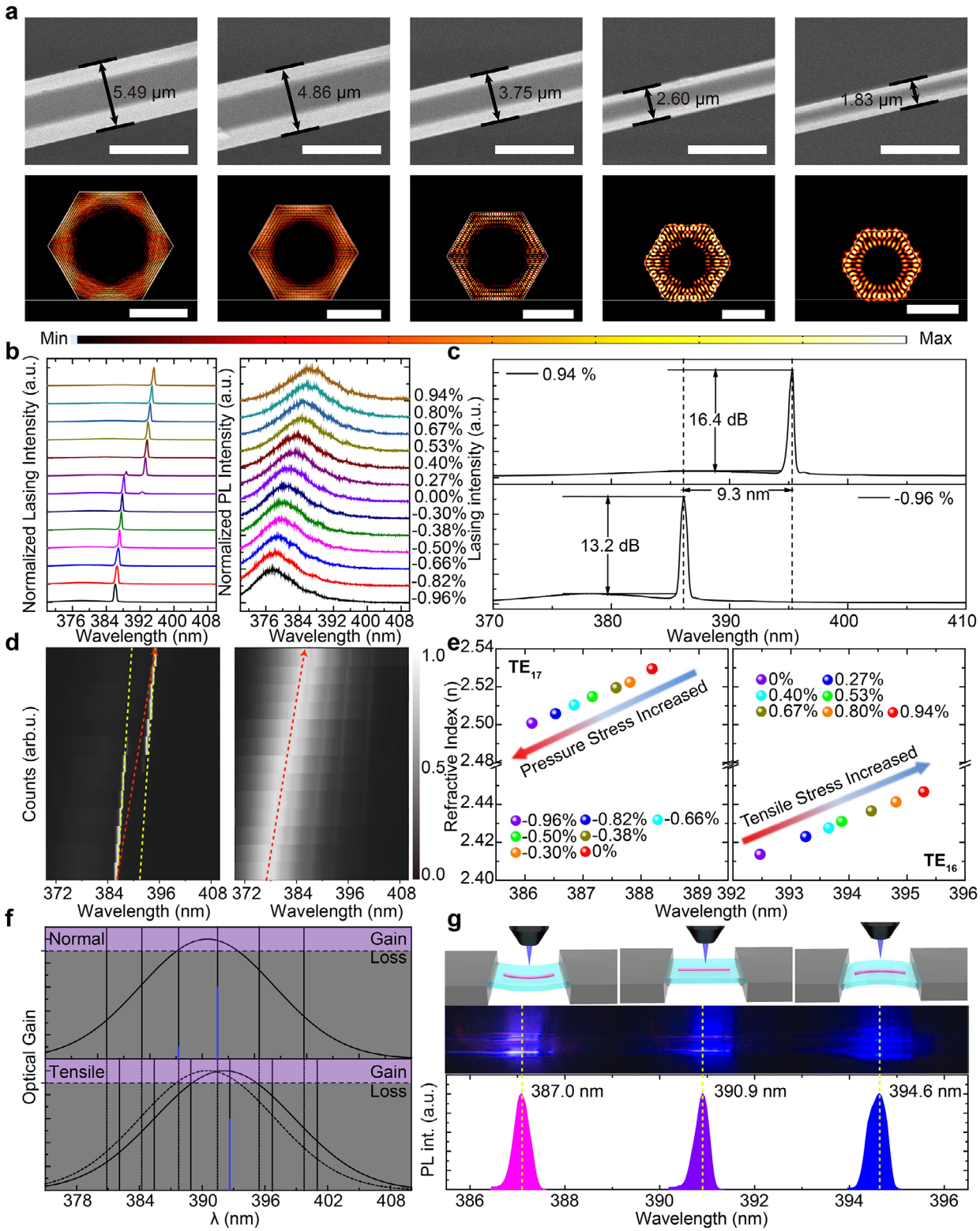

Figure 7. Single-mode lasing realization and dynamic regulation. a) SEM images (scale bars: 6 μm) and electric-field distribution (scale bars: 5, 3, 2, 1, and 1 μm, respectively) of the fundamental mode in simulated by FDTD method for different sized ZnO microrods; b) Lasing and PL spectra of the same ZnO microrod under different strains; c) lasing spectra of the same ZnO microrod under the strains of 0.94% and −0.96% with the SMSR of 16.4 dB and 13.2 dB; e) The relationship of refractive index and the wavelength of resonant mode under different strains; f) Regulation mechanism; g) Optical images and lasing spectra of the same stimulated ZnO microrod under three states of compressive, normal and tensile, respectively. Reproduced with permission.[146] Copyright 2018, Elsevier.

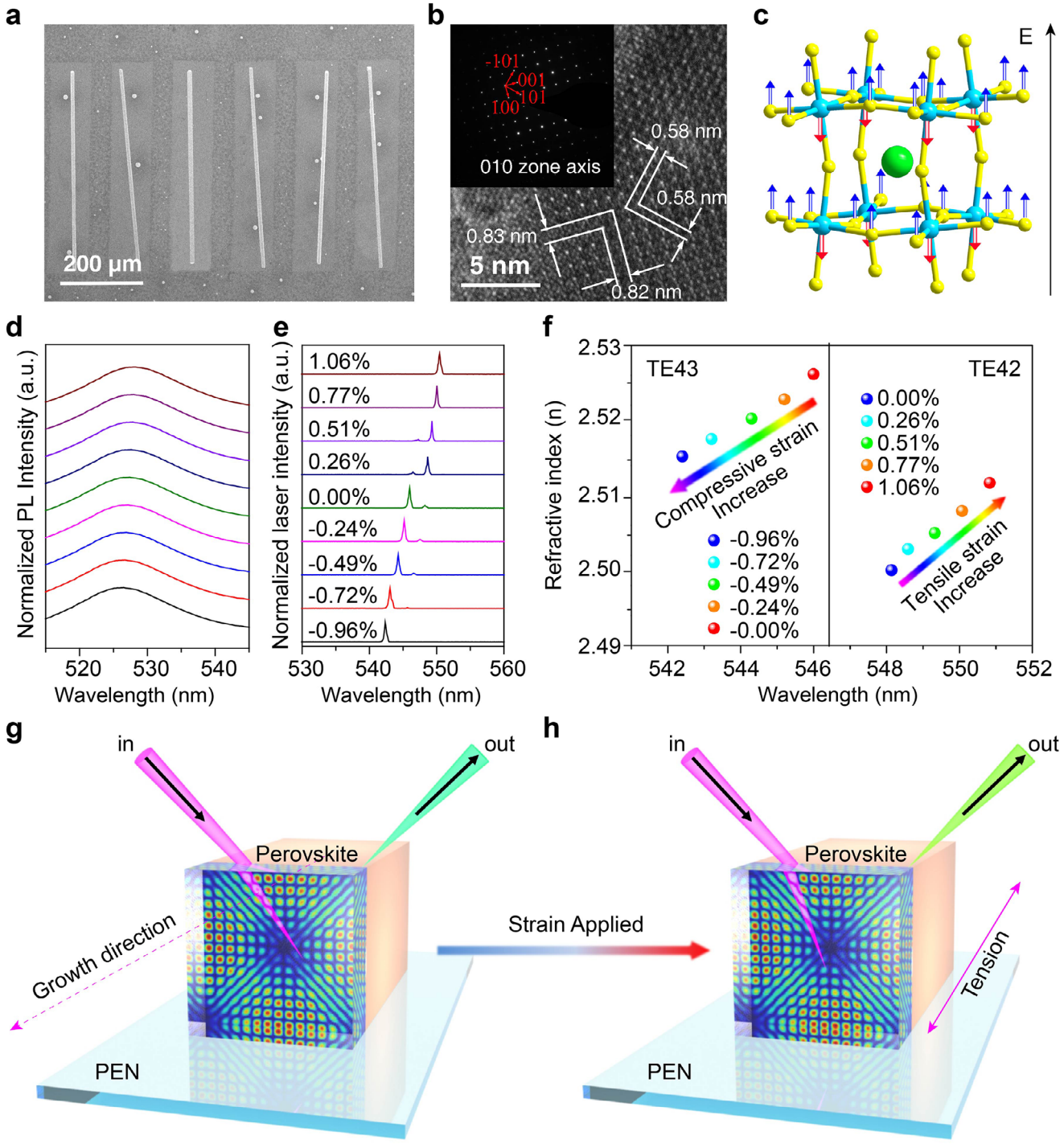

Figure 8. Dynamic regulation of lasing mode for an individual $CsPbBr_3$ microwire grown along [010] direction. a) SEM image of the aligned $CsPbBr_3$ microwires grown on the SiO_2/Si substrate. b) HRTEM image and the corresponding SEAD pattern of single $CsPbBr_3$ microwire. c) Schematic diagram of the perovskite cell polarization under the external strain. Lasing (e) and PL d) spectra for the $CsPbBr_3$ MW under the strain changing from −0.96% to 1.06%. f) The dependence of the resonant wavelengths for the TE_{43} and TE_{42} modes on the refractive index under different strains. Schematic diagrams of a $CsPbBr_3$ microcavity fixed on the PEN substrate operated from normal g) to tensile state h). Reproduced with permission.[156] Copyright 2019, John Wiley and Sons.

the 1960s, a lot of nonlinear optical phenomena represented by high-order harmonics, optical parametric amplification and oscillation (OPA and OPO), multiphoton absorption (MPA), optical sum-frequency and difference frequencies (SFG and DFG) have been observed in experiment successively.[157–160] At the beginning of the 20th century, nonlinear optical phenomena represented by multiphoton emission[161–163] were also observed in non-centrosymmetric wurtzite structural ZnO with a high optical damage threshold.

Figure 9a shows the schematic diagram of the vibration for A_{1TO} and E_{2H} phonon modes, the former being parallel to the *c* axis of ZnO, while the latter being perpendicular to the *c* axis of ZnO. In order to systematically analyze the lattice vibration and structural characteristics of ZnO, we performed the Raman measurement of the different angle between the polarization directions of incident light and the ZnO axial direction. The measurement setup is shown in Figure 8d, where the polarization directions can be controlled by rotating half-wave plate. Figure 9b,e demonstrates the 2D-color plots of angle-dependent Raman spectra for the same ZnO microrod under the tensile strain of 0.0% and 0.50%. The insets are the dependence of Raman intensity of E_{2L} and E_{2H} phonon modes on the polarized angle of θ. As $\theta = 90°$ and 270°, the strongest Raman intensity of E_{2L} and E_{2H} phonon modes can be observed both in the normal and tensile states. When $\theta = 0°$ and 180°, Raman intensity of E_{2L} and E_{2H} phonon modes becomes the weakest, indicating that these two phonon modes vibrated perpendicular to the c axis of ZnO have strong polarization dependence for incident light. Also, Raman spectra for the same ZnO microrod under different tensile strains, changing from 0% to 0.50% have been measured, as shown in Figure 9c. The obvious variation in the oscillation frequency of E_{2L} and E_{2H} phonon modes can be observed, while the vibration frequency of A_{1TO} phonon mode remains unchanged, as shown in Figure 9f. According to the classic atomic model, we compare the oscillation frequency of A_{1TO} phonon mode before and after the external force applied along in the c-axis direction of ZnO microrod, which is exactly the same. It reveals that wurtzite-structural ZnO has typical structural asymmetry, providing direct evidence for the generation of an electric dipole moment under external mechanical strain. Meanwhile, it also proposes a theoretical possibility for the successful observation of nonlinear optical phenomena in ZnO. Figure 9g,h shows the 2D-color plots and line graph of lasing spectra pumped by ≈710 nm femtosecond laser, with a lasing threshold of 15 μW. The FWHM is ≈0.12 nm at a pumping power of 15.5 μW. Therefore, the *Q* factor can be estimated as 3200 by the formula of $Q = \lambda/\delta\lambda$. Figure 8i shows the dependence of PL intensity on the pumping at different excited wavelength of 355, 650, 710, and 730 nm, respectively. The input-output relationship can be fitted by a power exponential function of $I \propto P^{\gamma}$ with the power-law exponent γ of 1.05, 1.89, 1.94 and 2.06, respectively. It implies that when the excitation photon energy is lower than the ZnO band gap, the energy of two photons must be absorbed simultaneously to complete the transition of an electron from the valence band to conduction band, as shown in the inset of Figure 9h. Subsequently, a home-made acrylic setup was used to apply uniaxial tensile strain to the ZnO microrods fixed on a flexible substrate, as shown in Figure 9j. As the tensile strain increases from 0% to 0.67%, an obvious redshift of TE mode can be observed in Figure 9k. Figure 9l demonstrates the dependence of the refractive index for TE_{33} and TE_{32} mode on the tensile strains. The change in refractive index is still the dominant factor in mode shift, which indicates that the mode regulation by utilizing this method has certain universality.[164] It provides an effective strategy for achieving high-quality mode-adjustable frequency up-conversion lasers.

6. The Potential Application in Strain Sensor by the Lasing Mode-Shift

As an essential component in all kinds of intelligent terminals (ITs), stress sensors have been investigated and developed extensively due to their potential application in life sciences, electronic skin, human health monitoring, and human-machine interaction. Many significant progresses in stress sensors based on different physical mechanisms, including capacitive, piezoresistive, and piezoelectric have been reported.[165–167] As reviewed in the above sections, the external mechanical strain can be used to dynamically modulate the lasing mode in the asymmetric central structural semiconductor materials, such as ZnO, GaN, CdS, and orthorhombic perovskite. Conversely, the amount of mode-shift also reflects the magnitude of the applied external force, which has an important potential application for strain sensing. In particular, GaN materials have achieved great success in the field of optoelectronic lighting, and forming a stable industrial structure. Meanwhile, it also has the advantages of good chemical stability and easy integration with existing Micro&Nano processing technology, which makes it an excellent candidate for building GaN-based strain sensors. Compared with the traditional changes in luminous intensity for stress sensing, it can eliminate interference from various external factors and improve the accuracy of detection by using wavelength shifting for stress detection.[136]

Figure 10a shows the Schematic diagram of the dynamically modulated GaN lasing mode under externally applied strain. Under the same tensile strain, the amount of PL movement is $\Delta\lambda'$, and the amount of lasing mode-shift is $\Delta\lambda$. It can be seen that the PL spectra before and after the applied strain still mostly overlap and are difficult to resolve, while the lasing mode is completely distinguished due to its ultra-narrow linewidth, revealing an ultra-high stress detection resolving capacity. In order to more intuitively illustrate the higher resolution of the stress detection through the shift of lasing mode, we have established a theoretical model, as shown in Figure 10b. In general, the line profile of lasing mode satisfies the Lorentz distribution, which can be fitted with the following function:

$$y = y_0 + \frac{2A}{\pi} \cdot \frac{\Delta\omega}{4\left(x - X_c\right)^2 + \Delta\omega^2} \tag{11}$$

where y_0, $\Delta\omega$ and X_c represent the asymptotic line, FWHM and the dominant wavelength of the fitting curve respectively, and *A* is a constant.

In Equation (11), if assigning x to $X_c \pm \Delta H$, where ΔH is the overlap in wavelength of the two lasing peaks. The function value y_1 shown in Figiure 10b can be expressed as:

$$y_1 = y_0 + \frac{2A}{\pi} \cdot \frac{\Delta\omega}{4\Delta H^2 + \Delta\omega^2} \tag{12}$$

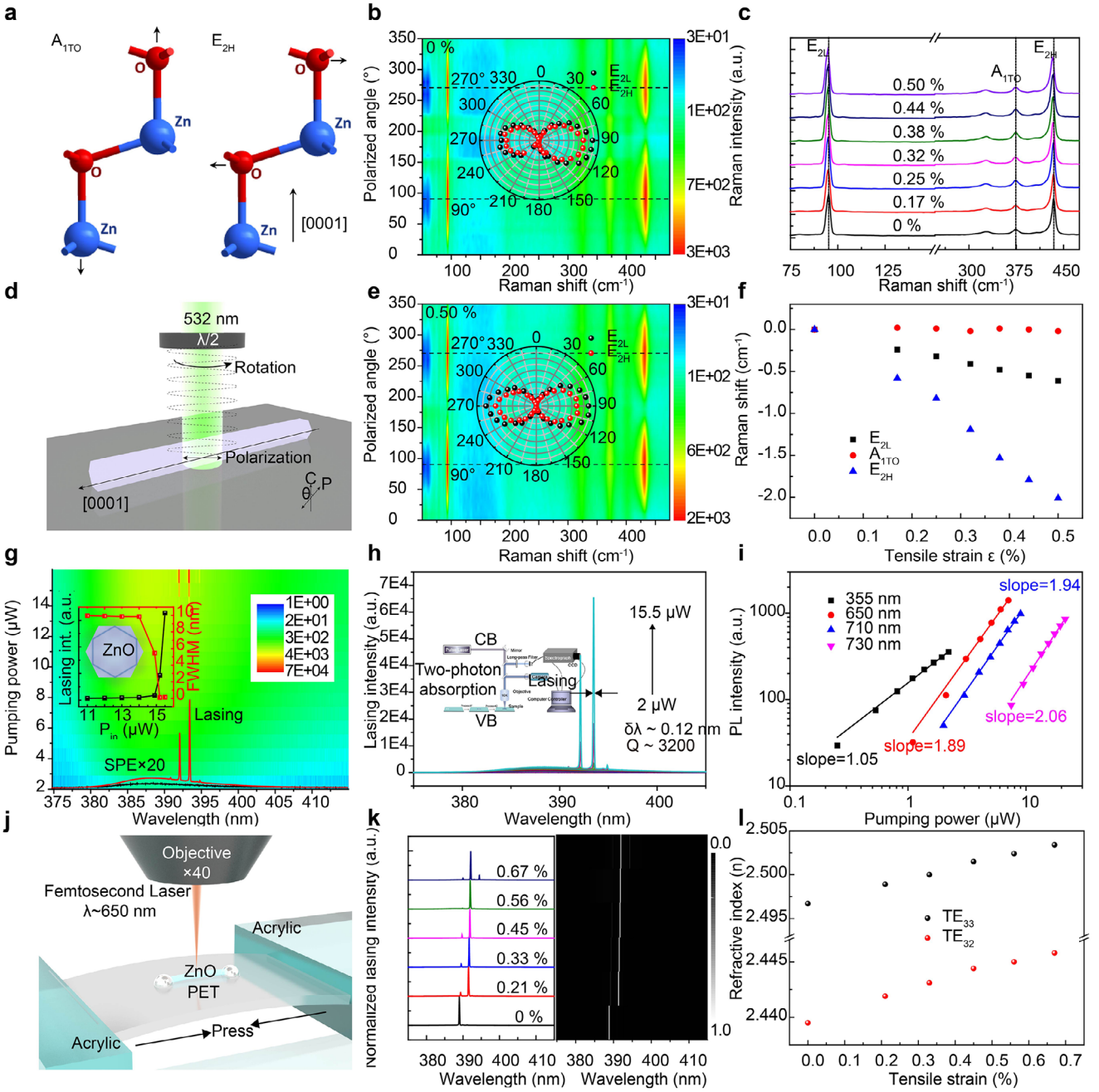

Figure 9. Two-photon pumped ZnO WGM lasing and mode regulation. a) Schematic diagram of A_{1TO}, E_{2H} phonon mode oscillation and d) Raman measurement for wurtzite-structural ZnO; b,e) Dependence of polarizing angle and Raman peaks shown by 2D color-plots under the tensile strain of 0% and 0.50%, inset: the corresponding integrated polar graph; c) Raman spectra of the same ZnO microrods under different tensile strains; f) The dependence of phonon frequency shifts of E_{2L}, E_{2H} and A_{1TO} on the applied strains; g) lasing spectra of ZnO microrod with increasing of pumping power shown by 2D color-plots, inset: the relationship of lasing intensity and FWHM with the pumping power; h) lasing spectra of ZnO microrod under different pumping power from 2 to 15.5 μW, inset: schematic diagram of two-photon-pumped transition mechanism; i) the relationship between integrated PL intensity and pumping power at different excitation wavelengths of 355, 650, 710 and 730 nm; j) schematic diagram of stress application and spectrum acquisition setup; k) lasing spectra and mappings under the different tensile strains changing from 0% to 0.67%; l) the dependence of the refractive index on the applied strain for TE_{33} and TE_{32} mode. Reproduced with permission.[164] Copyright 2019, John Wiley and Sons.

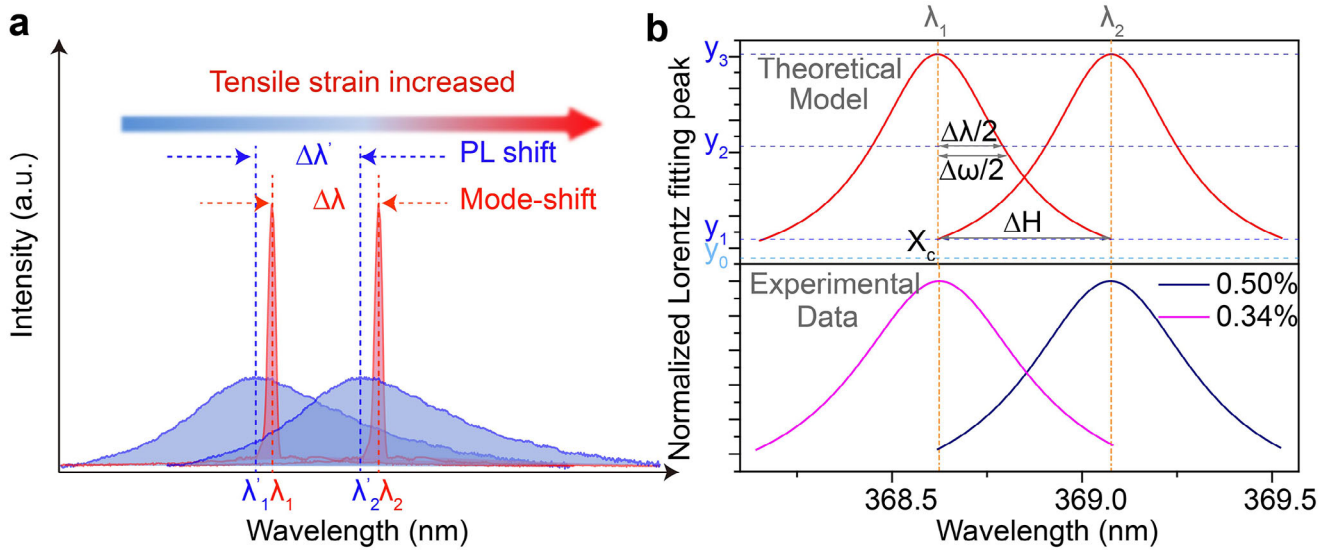

Figure 10. Quantitative analysis. a) Schematic diagram of dynamic control of GaN lasing mode and gain spectrum. b) Schematic diagram quantitatively illustrating the sensor color-resolving ability R. Reproduced with permission.[136] Copyright 2019, John Wiley and Sons.

If assigning x to $X_c \pm \Delta\lambda/2$, the function value y_2 shown in Figure 10b can be expressed as:

$$y_2 = y_0 + \frac{2A}{\pi} \cdot \frac{\Delta\omega}{\Delta\lambda^2 + \Delta\omega^2} \tag{13}$$

When x is the dominant wavelength of X_c, the function value y_3 shown in Figure 10b can be expressed as:

$$y_3 = y_0 + \frac{2A}{\pi} \cdot \frac{1}{\Delta\omega} \tag{14}$$

Here,

$$y_2 = \frac{y_1 + y_3}{2} \tag{15}$$

Substituting the value of y_1, y_2, and y_3 into Equation (15), we can get:

$$\frac{1}{\Delta\omega^2} + \frac{1}{4\Delta H^2 + \Delta\omega^2} = \frac{2}{\Delta\lambda^2 + \Delta\omega^2} \tag{16}$$

By simplification, the following relation formula can be derived:

$$\frac{1}{\Delta H^2} = \frac{2}{\Delta\lambda^2} - \frac{2}{\Delta\omega^2} \tag{17}$$

Subsequently, the factor of R is used to reflect the detection resolution of the stress sensor, which can be defined as:

$$R = \left| \frac{\lambda_2 - \lambda_1}{\Delta H} \right| \tag{18}$$

where λ_1 and λ_2 are the resonant wavelengths of lasing modes before and after applying the tensile strain, respectively. ΔH is the overlap region of the two lasing modes, which also satisfies the Equation (17). When the value of R factor is 1, it represents a critical state in which the two lasing mode peaks before and after the force applied can be resolved. In this case, the two resonant modes under tensile strain of 0.34% and 0.50% have been used to analyze the strain required to reach a critical state, as shown in below panel of Figure 10b. It can be seen that the two lasing modes have just been resolved as the strain changes from 0.34% to 0.50%, indicating that the stress detection capability through mode shift can be as low as 0.16%. Also, we estimate that the strain required to reach the critical state is about 0.14%, which is consistent with the experimental value of 0.16%, according to the theoretical model and the dependence of the mode resonance wavelength on the applied strain. It can be seen from Equation (17) that a narrower line width ($\Delta\lambda$) can obtain fewer spectral line overlap regions (ΔH), thereby achieving higher stress detection resolution (R). In addition, the detection sensitivity (S) and detection capability (C)[168] can be used to evaluate the performance of a strain sensor, which can be defined as $S = \Delta E/\varepsilon$ and $C = S/\Delta\lambda$, respectively, where ΔE is the photon energy difference under different strains, ε is the strain value, $\Delta\lambda$ is FWHM. The values of these two parameters are estimated to be 31.28 meV/% and 10.32%, respectively, revealing excellent sensing performance. In this work, due to the ultra-narrow line width of the lasing mode, the ability to perform stress detection through the mode-shift is an order of magnitude better than that by using PL movement.

7. Summary and Outlook

In summary, a new approach for selecting and tuning multi/single-mode lasing output dynamically in need of predesigned cavity configurations has been proposed through the synergistic effect of piezoelectricity and piezoresistivity in different materials systems, which has potential applications in constructing optical mode-phase modulator, highly sensitive optical switches, and color-perceived optical sensing. Moreover, the roles

of these two physical effects in the shift of the optical gain region and cavity modes are systematically investigated, which can also be extended to the dynamic modulation of two-photon pumped frequency up-conversion laser mode. On the other hand, it opens up exciting avenues for the design of high-precision, highly sensitive and non-contact flexible strain sensor, and may further apply on high-resolution imaging of pressure distributions by perceiving the color change of light emission. In addition, it provides an excellent platform to explore many important physical processes such as the generation and recombination of electron-hole pairs, light-matter interactions, and cavity quantum electrodynamics in microcavities under the action of piezoelectric fields.

However, there are still numerous challenges to meet practical application requirements. For example, the dynamically tuning range of the resonant wavelength of the lasing mode is relatively small under the external mechanical strain, and it is still difficult for the human eye to recognize the color difference. Secondly, the method of dynamic, continuous, and reversible regulation of the lasing mode is relatively simple in this review. It mainly used the effect of external strain on the refractive index of the cavity to achieve the objective. It is needed to develop more regulatory approaches to address the actual needs of different environments. Meanwhile, in order to realize high-resolution pressure mapping through color change perception, it is necessary to prepare the high crystal quality optical resonator arrays, which place higher requirements on the material growth process. At present, the development of this novel dynamic modulation method of lasing mode reviewed in this paper is still in its preliminary stage, in which challenges and opportunities coexist. We firmly believe that it will usher in a bright application prospect.

Acknowledgements

The authors thank the support of the Fundamental Research Funds for the Central Universities (No. NS2024063), National Natural Science Foundation of China (Nos. 52572172, 61805015, 62105035, 52125205, 52250398, U20A20166, 12374257, 52192614 and 52003101), the Natural Science Foundation of Jiangsu Province (BK20231441) and the Open Fund of the National Key Laboratory of Solid Microstructure Physics, Nanjing University (M38042), National Key Research and Development Program of China (2021YFB3200300), Natural Science Foundation of Beijing Municipality (2222088), Shenzhen Science and Technology Program (Grant No. KQTD20170810105439418) and the Fundamental Research Funds for the Central Universities.

Conflict of Interest

The authors declare no conflict of interest.

Keywords

laser, mode regulation, piezoelectric effect, piezoresistive effect, strain sensors

Received: July 17, 2025
Revised: September 30, 2025
Published online:

[1] T. H. Maiman, *Nature* **1960**, *187*, 493.
[2] G. Field, D. Spergel, *Science* **1986**, *231*, 1387.
[3] A. D. McAulay, *Military Laser Technology for Defense: Technology for Revolutionizing 21st Century Warfare*, John Wiley & Sons, Hoboken, NJ, USA **2011**.
[4] J. L. Marx, *Science* **1975**, *188*, 821.
[5] V. V. Tuchin, *Laser Phys.* **1993**, *3*, 767;
[6] D. Burkhoff, S. Schmidt, S. P. Schulman, J. Myers, J. Resar, L. C. Becker, J. Weiss, J. W. Jones, *Lancet* **1999**, *354*, 885.
[7] A. C. Keech, P. Mitchell, P. A. Summanen, J. O'Day, T. M. E. Davis, M. S. Moffitt, M. R. Taskinen, R. J. Simes, D. Tse, E. Williamson, A. Merrifield, L. T. Laatikainen, M. C. d'Emden, D. C. Crimet, R. L. O'Connell, P. G. Colman, *Lancet* **2007**, *370*, 1687.
[8] C. F. Lin, Y. S. Su, B. R. Wu, *IEEE Photonic Tech. L* **2002**, *14*, 3.
[9] E. Murphy, *Nat. Photonics* **2010**, *4*, 287.
[10] H. Al-Taiy, N. Wenzel, S. Preußler, J. Klinger, T. Schneider, *Opt. Lett.* **2014**, *39*, 5826.
[11] R. C. Crafer, P. J. Oakley, *Laser Processing in Manufacturing*, Chapman & Hall, London, UK **1993**.
[12] M. C. Gower, *Opt. Express* **2000**, *7*, 56.
[13] Y. L. Zhang, Q. D. Chen, H. Xia, H. B. Sun, *Nano Today* **2010**, *5*, 435. .
[14] S. F. Wu, S. Buckley, J. R. Schaibley, L. F. Feng, J. Q. Yan, D. G. Mandrus, F. Hatami, W. Yao, J. Vučković, A. Majumdar, X. D. Xu, *Nature* **2015**, *520*, 69;
[15] R. Köhler, A. Tredicucci, F. Beltram, H. E. Beere, E. H. Linfield, A. G. Davies, D. A. Ritchie, R. C. Iotti, F. Rossi, *Nature* **2002**, *417*, 156;
[16] I. D. W. Samuel, G. A. Turnbull, *Chem. Rev.* **2007**, *107*, 1272.
[17] C. Gmachl, D. L. Sivco, R. Colombelli, F. Capasso, A. Y. Cho, *Nature* **2002**, *415*, 883.
[18] M. Beck, D. Hofstetter, T. Aellen, J. Faist, U. Oesterie, M. Llegems, E. Gini, H. Melchior, *Science* **2002**, *295*, 301.
[19] A. Uchida, K. Amano, M. Inoue, K. Hirano, S. Naito, H. Someya, I. Oowada, T. Kurashige, M. Shiki, S. Yoshimori, K. Yoshimura, P. Davis, *Nat. Photonics* **2008**, *2*, 728.
[20] F. Qian, Y. Li, S. Gradečak, H. G. Park, Y. J. Dong, Y. Ding, Z. L. Wang, C. M. Lieber, *Nat. Mater.* **2008**, *7*, 701;
[21] A. L. Pan, W. C. Zhou, E. S. P. Leong, R. B. Liu, A. H. Chin, B. S. Zou, C. Z. Ning, *Nano Lett.* **2009**, *9*, 784.
[22] H. Zong, Y. Yang, C. Ma, X. H. Feng, T. T. Wei, W. Yang, J. C. Li, J. Z. Li, L. P. You, J. Zhang, M. Li, C. F. Pan, X. D. Hu, B. Chen, *ACS Nano* **2017**, *11*, 5808.
[23] Z. Y. Yang, D. L. Wang, C. Meng, Z. M. Wu, Y. Wang, Y. G. Ma, L. Dai, X. W. Liu, T. Hasan, X. Liu, Q. Yang, *Nano Lett.* **2014**, *14*, 3153.
[24] W. Q. Wu, H. Lu, X. Han, C. F. Wang, Z. S. Xu, S. T. Han, C. F. Pan, *Small Methods* **2023**, *7*, 2201499.
[25] J. B. Li, C. Meng, Y. Liu, X. Q. Wu, Y. Z. Lu, Y. Ye, L. Dai, L. M. Tong, X. Liu, Q. Yang, *Adv. Mater.* **2013**, *25*, 833.
[26] X. F. Liu, Q. Zhang, Q. H. Xiong, T. C. Sum, *Nano Lett.* **2013**, *13*, 1080.
[27] Q. Zhang, Q. Y. Shang, J. Shi, J. Chen, R. Wang, Y. Mi, W. N. Du, C. Shen, R. M. Ma, X. H. Qiu, X. F. Liu, T. C. Sum, *ACS Photonics* **2017**, *4*, 2789.
[28] X. D. Wang, Z. Z. Li, M. P. Zhuo, Y. S. Wu, S. Chen, J. N. Yao, H. B. Fu, *Adv. Funct. Mater.* **2017**, *27*, 1703470.
[29] X. F. Liu, Q. Zhang, J. N. Yip, Q. H. Xiong, T. C. Sum, *Nano Lett.* **2013**, *13*, 5336.
[30] E. Burstein, *Phys. Rev.* **1954**, *93*, 632.
[31] T. S. Moss, *Proc. Phys. Soc. B* **1954**, *67*, 775.
[32] J. T. Li, Y. Lin, J. F. Lu, C. X. Xu, Y. Y. Wang, Z. L. Shi, J. Dai, *ACS Nano* **2015**, *9*, 6794.
[33] D. J. Gargas, M. C. Moore, A. Ni, S. W. Chang, Z. Y. Zhang, S. L. Chuang, P. D. Yang, *ACS Nano* **2010**, *4*, 3270.

[34] Q. M. Li, J. B. Wright, W. W. Chow, T. S. Luk, L. Brener, L. F. Lester, G. T. Wang, *Opt. Express* **2012**, *20*, 17873.
[35] D. C. Hanna, B. Luther-Davies, R. C. Smith, *Electron. Lett.* **1972**, *8*, 369.
[36] D. T. Nichols, J. Lopata, W. S. Hobson, P. F. Sciortino, N. K. Dutta, *Electron. Lett.* **1993**, *29*, 2035.
[37] M. P. Nesnidal, L. J. Mawst, A. Bhattacharya, D. Botez, L. DiMarco, J. C. Connolly, J. H. Abeles, *IEEE Photonic. Tech. L.* **1996**, *8*, 182.
[38] H. P. Gauggel, R. Winterhoff, J. Kuhn, F. Scholz, H. Schweizer, *Electron. Lett.* **1997**, *33*, 1466.
[39] Y. Y. Wang, C. X. Xu, M. M. Jiang, J. T. Li, J. Dai, J. F. Lu, P. L. Li, *Nanoscale* **2016**, *8*, 16631.
[40] H. W. Gao, A. Fu, S. C. Andrews, P. D. Yang, *P. Natl. Acad, Sci.* **2013**, *110*, 865.
[41] W. Lee, H. Li, J. D. Suter, K. Reddy, Y. Z. Sun, X. D. Fan, *Appl. Phys. Lett.* **2011**, *98*, 061103.
[42] Y. Xiao, C. Meng, P. Wang, Y. Ye, H. Yu, S. S. Wang, F. X. Gu, L. Dai, L. M. Tong, *Nano Lett.* **2011**, *11*, 1122.
[43] L. Feng, Z. J. Wong, R. M. Ma, Y. Wang, X. Zhang, *Science* **2014**, *346*, 972.
[44] P. Miao, Z. F. Zhang, J. B. Sun, W. Walasik, S. Longhi, N. M. Litchinitser, L. Feng, O. microlaser, *Science* **2016**, *353*, 464.
[45] H. Hodaei, M. A. Miri, M. Heinrich, D. N. Christodoulides, M. Khajavikhan, *Science* **2014**, *346*, 975.
[46] B. Peng, Ş. K. Özdemir, F. C. Lei, F. Monifi, M. Gianfreda, G. L. Long, S. H. Fan, F. Nori, C. M. Bender, L. Yang, *Nat. Phys.* **2014**, *10*, 394.
[47] F. X. Gu, F. M. Xie, X. Lin, S. Y. Linghu, W. Fang, H. P. Zeng, L. M. Tong, S. L. Zhuang, *Light: Sci. Appl.* **2017**, *6*, 17061;
[48] S. F. Liew, B. Redding, L. Ge, G. S. Solomon, H. Cao, *Appl. Phys. Lett.* **2014**, *104*, 231108.
[49] M. H. Zhao, Z. L. Wang, S. X. Mao, *Nano Lett.* **2004**, *4*, 587.
[50] W. S. Su, Y. F. Chen, C. L. Hsiao, L. W. Tu, *Appl. Phys. Lett.* **2007**, *90*, 063110.
[51] Y. F. Lin, J. Song, Y. Ding, S. Y. Lu, Z. L. Wang, *Appl. Phys. Lett.* **2008**, *92*, 022105.
[52] Y. M. You, W. Q. Liao, D. W. Zhao, H. Y. Ye, Y. Zhang, Q. H. Zhou, X. H. Niu, J. L. Wang, P. F. Li, D. W. Fu, Z. M. Wang, S. Gao, K. L. Yang, J. M. Liu, J. Y. Li, Y. F. Yan, R. G. Xiong, *Science* **2017**, *357*, 306.
[53] M. L. Que, W. X. Guo, X. J. Zhang, X. Y. Li, Q. L. Hua, L. Dong, C. F. Pan, *J. Mater. Chem. A* **2014**, *2*, 13661.
[54] C. F. Wang, D. F. Peng, J. Zhao, R. R. Bao, T. Li, L. Tian, L. Dong, C. Y. Shen, C. F. Pan, *Small* **2016**, *12*, 5734.
[55] C. F. Pan, L. Dong, G. Zhu, S. M. Niu, R. M. Yu, Q. Yang, Y. Liu, Z. L. Wang, *Nat. Photonics* **2013**, *7*, 752.
[56] W. Z. Wu, X. N. Wen, Z. L. Wang, *Science* **2013**, *340*, 952.
[57] Y. Y. Peng, M. L. Que, H. E. Lee, R. R. Bao, X. D. Wang, J. F. Lu, Z. Q. Yuan, X. Y. Li, J. Tao, J. L. Sun, J. Y. Zhai, K. J. Lee, C. F. Pan, *Nano Energy* **2019**, *58*, 633.
[58] R. R. Bao, C. F. Wang, L. Dong, R. M. Yu, K. Zhao, Z. L. Wang, C. F. Pan, *Adv. Funct. Mater.* **2015**, *25*, 2884.
[59] C. F. Wang, C. F. Pan, Z. L. Wang, *ACS Nano* **2019**, *13*, 12287.
[60] R. R. Bao, J. Tao, J. Zhao, M. Dong, J. Li, C. F. Pan, *Sci. Bull.* **2023**, *68*, 1027.
[61] C. F. Wang, H. J. Hu, D. L. Zhu, C. F. Pan, *Sci. Bull.* **2023**, *68*, 559.
[62] W. Z. Wu, L. Wang, Y. L. Li, F. Zhang, L. Lin, S. M. Niu, D. Chenet, X. Zhang, Y. F. Hao, T. F. Heinz, J. Hone, Z. L. Wang, *Nature* **2014**, *514*, 470.
[63] R. S. Yang, Y. Qin, L. M. Dai, Z. L. Wang, *Nat. Nanotechnol.* **2009**, *4*, 34.
[64] R. S. Yang, Y. Qin, C. Li, G. Zhu, Z. L. Wang, *Nano Lett.* **2009**, *9*, 1201.
[65] M. Lee, C. Y. Chen, S. H. Wang, S. N. Cha, Y. J. Park, J. M. Kim, L. J. Chou, Z. L. Wang, *Adv. Mater.* **2012**, *24*, 1759.
[66] W. D. Ma, J. F. Lu, B. S. Wan, D. F. Peng, Q. Xu, G. F. Hu, Y. Y. Peng, C. F. Pan, Z. L. Wang, *Adv. Mater.* **2020**, *32*, 1905795.
[67] J. Tao, M. Dong, L. Li, C. F. Wang, J. Li, Y. Liu, R. R. Bao, C. F. Pan, *Microsystems&Nanoengineering* **2020**, *6*, 62;
[68] Z. Y. Chen, R. H. Zhou, J. Y. Huang, H. C. Xu, Z. M. Li, Y. S. Wang, R. R. Bao, J. He, C. F. Pan, *Adv. Funct. Mater.* **2024**, *34*, 2406434.
[69] Q. Yang, X. Guo, W. H. Wang, Y. Zhang, S. Xu, D. H. Lien, Z. L. Wang, *ACS Nano* **2010**, *4*, 6285.
[70] X. D. Wang, J. Zhou, J. H. Song, J. Liu, N. S. Xu, Z. L. Wang, *Nano Lett.* **2006**, *6*, 2768.
[71] X. Xiao, L. Y. Yuan, J. W. Zhong, T. P. Ding, Y. Liu, Z. X. Cai, Y. G. Rong, H. W. Han, J. Zhou, Z. L. Wang, *Adv. Mater.* **2011**, *23*, 5440.
[72] X. Han, W. M. Du, R. M. Yu, C. F. Cao, Z. L. Wang, *Adv. Mater.* **2015**, *27*, 7963.
[73] X. D. Wang, H. L. Zhang, R. M. Yu, L. Dong, D. F. Peng, A. H. Zhang, Y. Zhang, H. Liu, C. F. Pan, Z. L. Wang, *Adv. Mater.* **2015**, *27*, 2324.
[74] H. L. Zhang, D. F. Peng, W. Wang, L. Dong, C. F. Pan, *J. Phys. Chem. C* **2015**, *119*, 28136.
[75] H. Liu, Q. M. Li, Y. B. Bu, N. Zhang, C. F. Wang, C. F. Pan, L. W. Mi, Z. H. Guo, C. T. Liu, C. Y. Shen, *Nano Energy* **2019**, *66*, 104143.
[76] C. F. Wang, J. Zhao, C. Ma, J. L. Sun, L. Tian, X. Y. Li, F. T. Li, X. Han, C. T. Liu, C. Y. Shen, L. Dong, J. Yang, C. F. Pan, *Nano Energy* **2017**, *34*, 578.
[77] Y. h. Wu, L. B. Huang, C. F. Pan, *Sci. Bull.* **2023**, *68*, 1849.
[78] W. Q. Wu, C. F. Wang, S. T. Han, C. F. Pan, *Rare Met.* **2024**, *43*, 5487.
[79] Y. Liu, J. Tao, Y. P. Mo, R. R. Bao, C. F. Pan, *Adv. Mater.* **2024**, *36*, 2313857.
[80] R. H. Han, Y. Liu, Y. P. Mo, H. C. Xu, Z. W. Yang, R. R. Bao, C. F. Pan, *Adv. Funct. Mater.* **2023**, *33*, 2305531;
[81] G. C. Wu, X. Li, R. R. Bao, C. F. Pan, *Adv. Funct. Mater.* **2024**, *34*, 2405722.
[82] Z. L. Wang, *Adv. Mater.* **2012**, *24*, 280.
[83] S. Xu, Y. Qin, C. Xu, Y. G. Wei, R. S. Yang, Z. L. Wang, *Nat. Nanotechnol.* **2010**, *5*, 366;
[84] S. Xu, B. J. Hansen, Z. L. Wang, *Nat. Commun.* **2010**, *1*, 93.
[85] Y. F. Hu, Y. Zhang, C. Xu, L. Lin, R. L. Snyder, Z. L. Wang, *Nano Lett.* **2011**, *11*, 2572.
[86] Z. L. Wang, *Mater. Today* **2017**, *20*, 74;
[87] C. F. Pan, W. X. Guo, L. Dong, G. Zhu, Z. L. Wang, *Adv. Mater.* **2012**, *24*, 3356.
[88] K. K. Zhou, Y. Zhao, X. P. Sun, Z. Q. Yuan, G. Q. Zheng, K. Dai, L. W. Mi, C. F. Pan, C. T. Liu, C. Y. Shen, *Nano Energy* **2020**, *70*, 104546.
[89] Z. L. Wang, J. H. Song, *Science* **2006**, *312*, 242.
[90] J. H. He, C. L. Hsin, J. Liu, L. J. Chen, Z. L. Wang, *Adv. Mater.* **2007**, *19*, 781.
[91] J. L. Sun, Q. L. Hua, R. R. Zhou, D. M. Li, W. X. Guo, X. Y. Li, G. F. Hu, C. X. Shan, Q. B. Meng, L. Dong, C. F. Pan, Z. L. Wang, *ACS Nano* **2019**, *13*, 4507.
[92] Q. Yang, W. H. Wang, S. Xu, Z. L. Wang, *Nano Lett.* **2011**, *11*, 4012.
[93] Q. Xu, Z. Yang, D. F. Peng, J. G. Xi, P. Lin, Y. Cheng, K. H. Liu, C. Pan, *Nano Energy* **2019**, *65*, 104001.
[94] S. Qiao, J. H. Liu, G. S. Fu, K. L. Ren, Z. Q. Li, S. F. Wang, C. F. Pan, *Nano Energy* **2018**, *49*, 508.
[95] G. F. Hu, W. X. Guo, R. M. Yu, X. N. Yang, R. R. Zhou, C. F. Pan, Z. L. Wamg, *Nano Energy* **2016**, *23*, 27.
[96] R. R. Bao, C. F. Wang, Z. C. Peng, C. Ma, L. Dong, C. F. Pan, *ACS Photonics* **2017**, *4*, 1344.
[97] L. Dong, S. M. Niu, C. F. Pan, R. M. Yu, Y. Zhang, Z. L. Wang, *Adv. Mater.* **2012**, *24*, 5470.
[98] C. F. Wang, R. R. Bao, K. Zhao, T. P. Zhang, L. Dong, C. F. Pan, *Nano Energy* **2015**, *14*, 364.
[99] Z. L. Wang, *Adv. Mater.* **2007**, *19*, 889.

[100] Z. L. Wang, *Adv. Mater.* **2012**, *24*, 4632.
[101] Z. L. Wang, *Nano Today* **2010**, *5*, 540.
[102] Y. Zhang, Y. Liu, Z. L. Wang, *Adv. Mater.* **2011**, *23*, 3004.
[103] Z. L. Wang, *Mater. Today* **2007**, *10*, 20.
[104] R. M. Yu, L. Dong, C. F. Pan, S. M. Niu, H. F. Liu, W. Liu, S. Chua, D. Z. Chi, Z. L. Wang, *Adv. Mater.* **2012**, *24*, 3532.
[105] R. R. Bao, C. F. Wang, L. Dong, C. Y. Shen, K. Zhao, C. F. Pan, *Nanoscale* **2016**, *8*, 8078.
[106] K. Vedam, T. A. Davis, *Phys. Rev.* **1969**, *181*, 1196.
[107] C. S. Smith, *Phys. Rev.* **1954**, *94*, 42.
[108] X. W. Fu, Z. M. Liao, R. Liu, F. Lin, J. Xu, R. Zhu, W. Zhong, Y. K. Liu, W. L. Guo, D. P. Yu, *ACS Nano* **2015**, *9*, 11960.
[109] X. B. Han, L. Z. Kou, X. L. Lang, J. B. Xia, N. Wang, R. Qin, J. Lu, J. Xu, Z. M. Liao, X. Z. Zhang, X. D. Shan, X. F. Song, J. Y. Gao, W. L. Guo, D. P. Yu, *Adv. Mater.* **2009**, *21*, 4937.
[110] X. B. Han, L. Z. Kou, Z. H. Zhang, Z. Y. Zhang, X. L. Zhu, J. Xu, Z. M. Liao, W. L. Guo, D. P. Yu, *Adv. Mater.* **2012**, *24*, 4707.
[111] X. W. Fu, C. Su, Q. Fu, X. L. Zhu, R. Zhu, C. P. Liu, Z. M. Liao, J. Xu, W. L. Guo, J. Feng, J. Li, D. P. Yu, *Adv. Mater.* **2014**, *26*, 2572.
[112] W. Shan, T. J. Schmidt, R. J. Hauenstein, J. J. Song, *Appl. Phys. Lett.* **1995**, *66*, 3492.
[113] Q. Fu, Z. Y. Zhang, L. Z. Kou, P. C. Wu, X. B. Han, X. L. Zhu, J. Y. Gao, J. Xu, Q. Zhao, W. L. Guo, D. P. Yu, *Nano Res.* **2011**, *4*, 308.
[114] A. E. Siegman, *Lasers*, University Science Books, New York **1986**.
[115] T. Nobis, E. M. Kaidashev, A. Rahm, M. Lorenz, M. Grundmann, *Phys. Rev. Lett.* **2004**, *93*, 103903.
[116] J. Wiersig, *Phys. Rev. A* **2003**, *67*, 023807.
[117] Y. D. Yang, Y. Z. Huang, *J. Phys. D: Appl. Phys.* **2016**, *49*, 253001.
[118] W. H. Guo, Y. Z. Huang, Q. Y. Lu, L. J. Yu, *IEEE J. Quantum Elect.* **2003**, *39*, 1106.
[119] J. F. Lu, C. X. Xu, J. Dai, J. T. Li, Y. Y. Wang, Y. Lin, P. L. Li, *Nanoscale* **2015**, *7*, 3396.
[120] J. F. Lu, M. M. Jiang, M. Wei, C. X. Xu, S. F. Wang, Z. Zhu, F. F. Qin, Z. L. Shi, C. F. Pan, *ACS Photonics* **2017**, *4*, 2419.
[121] J. F. Lu, C. X. Xu, H. Y. Nan, Q. X. Zhu, F. F. Qin, A. G. Manohari, M. Wei, Z. Zhu, Z. L. Shi, Z. H. Ni, *Appl. Phys. Lett.* **2016**, *109*, 073701.
[122] J. F. Lu, J. T. Li, C. X. Xu, Y. Li, J. Dai, Y. Y. Wang, Y. Lin, S. F. Wang, *ACS Appl. Mater. Interfaces* **2014**, *6*, 18301.
[123] S. Chu, G. P. Wang, W. H. Zhou, Y. Q. Lin, L. Chernyak, J. Zhao, J. Y. Kong, L. Li, J. J. Ren, J. L. Liu, *Nat. Nanotechnol.* **2011**, *6*, 506;
[124] H. Zhu, C. X. Shan, J. Y. Zhang, Z. Z. Zhang, B. H. Li, D. X. Zhao, B. Yao, D. Z. Shen, X. W. Fan, Z. K. Tang, X. H. Hou, K. L. Choy, *Adv. Mater.* **2010**, *22*, 1877;
[125] J. Dai, C. X. Xu, X. W. Sun, *Adv. Mater.* **2011**, *23*, 4115.
[126] H. Cao, Y. G. Zhao, S. T. Ho, E. W. Seelig, Q. H. Wang, R. P. H. Chang, *Phys. Rev. Lett.* **1999**, *82*, 2278.
[127] M. H. Huang, S. Mao, H. Feick, H. Q. Yan, Y. Y. Wu, H. Kind, E. Weber, R. Russo, P. D. Yang, *Science* **2001**, *292*, 1897;
[128] C. X. Xu, J. Dai, G. Y. Zhu, Y. Lin, J. T. Li, Z. L. Shi, *Laser Photonics Rev.* **2014**, *8*, 469.
[129] J. F. Lu, C. X. Xu, J. Dai, J. T. Li, Y. Y. Wang, Y. Lin, P. L. Li, *ACS Photonics* **2015**, *2*, 73.
[130] C. X. Xu, F. F. Qin, Q. X. Zhu, J. F. Lu, Y. Y. Wang, J. T. Li, Y. Lin, Q. N. Cui, Z. L. Shi, A. G. Manohari, *Nano Res.* **2018**, *11*, 3050;
[131] J. F. Lu, Q. X. Zhu, Z. Zhu, Y. J. Liu, M. Wei, Z. L. Shi, C. X. Xu, *J. Mater. Chem. C* **2016**, *4*, 7718.
[132] J. F. Lu, C. X. Xu, F. T. Li, Z. Yang, Y. Y. Peng, X. Y. Li, M. L. Que, C. F. Pan, Z. L. Wang, *ACS Nano* **2018**, *12*, 11899.
[133] Q. S. Chen, Y. Y. Peng, F. T. Li, W. D. Ma, M. H. Zhuge, W. Q. Wu, J. L. Sun, X. H. Yang, J. F. Lu, C. F. Pan, *Nanotechnology* **2020**, *31*, 225202.
[134] Z. X. Shi, T. C. Shen, L. Dou, Z. Q. Gu, R. L. Zhu, X. Y. Dong, F. X. Gu, *Laser Photonics Rev.* **2024**, *18*, 2400384.
[135] R. L. Zhu, Z. Q. Gu, T. C. Shen, Y. F. Liu, Z. X. Shi, S. Y. Linghu, F. X. Gu, *Laser Photonics Rev.* **2025**, e02268, https://doi.org/10.1002/lpor.202402268.
[136] Y. Y. Peng, J. F. Lu, D. F. Peng, W. D. Ma, F. T. Li, Q. S. Chen, X. D. Wang, J. L. Sun, H. T. Liu, C. F. Pan, *Adv. Funct. Mater.* **2019**, *29*, 1905051.
[137] W. D. Ma, J. F. Lu, Z. Yang, D. F. Peng, F. T. Li, Y. Y. Peng, Q. S. Chen, J. L. Sun, J. G. Xi, C. F. Pan, *ACS Nano* **2019**, *13*, 5049.
[138] G. D. Mahan, J. J. Hopfield, *Phys. Rev. Lett.* **1964**, *12*, 241.
[139] M. Zapf, R. Röder, K. Winkler, L. Kaden, J. Greil, M. Wille, M. Grundmann, R. Schmidt-Grund, A. Lugstein, C. Ronning, *Nano Lett.* **2017**, *17*, 6637.
[140] C. Grivas, C. Y. Li, P. Andreakou, P. F. Wang, M. Ding, G. Brambilla, L. Manna, P. Lagoudakis, *Nat. Commun.* **2013**, *4*, 2376.
[141] J. F. Lu, W. Liu, M. M. Jiang, X. B. Zhou, J. Xu, Y. Liu, C. X. Kan, D. N. Shi, C. X. Xu, *Appl. Phys. Lett.* **2021**, *119*, 131103.
[142] H. W. Xu, J. B. Wright, T. S. Luk, J. J. Figiel, K. Cross, L. F. Lester, G. Balakrishnan, G. T. Wang, I. Brener, Q. M. Li, *Appl. Phys. Lett.* **2012**, *101*, 113106.
[143] Y. Xiao, C. Meng, X. Q. Wu, L. M. Tong, *Appl. Phys. Lett.* **2011**, *99*, 023109.
[144] W. L. Liu, M. Li, R. S. Guzzon, E. J. Norberg, J. S. Parker, M. Z. Lu, L. A. Coldren, J. P. Yao, *Nat. Commun.* **2017**, *8*, 15389.
[145] B. Pezeshki, J. S. Osinski, H. Zhao, A. Mathur, T. L. Koch, *Electron. Lett.* **1996**, *32*, 2241.
[146] J. F. Lu, Z. Yang, F. T. Li, M. M. Jiang, Y. F. Zhang, J. L. Sun, G. F. Hu, Q. Xu, C. X. Xu, C. F. Pan, Z. L. Wang, *Mater. Today* **2019**, *24*, 33.
[147] H. M. Zhu, Y. P. Fu, F. Meng, X. X. Wu, Z. Z. Gong, Q. Ding, M. V. Gustafsson, M. T. Tribh, S. Jin, X. Y. Zhu, *Nat. Mater.* **2015**, *14*, 636;
[148] G. C. Xing, N. Mathews, S. S. Lim, N. Yantara, X. F. Liu, D. Sabba, M. Grätzel, S. Mhaisalkar, T. C. Sum, *Nat. Mater.* **2014**, *13*, 476.
[149] Y. F. Jia, R. A. Kerner, A. J. Grede, B. P. Rand, N. C. Giebink, *Nat. Photonics* **2017**, *11*, 784.
[150] J. Z. Song, J. H. Li, X. M. Li, L. M. Xu, Y. H. Dong, H. B. Zeng, *Adv. Mater.* **2015**, *27*, 7162.
[151] R. Ding, X. L. Zhang, X. W. Sun, *Adv. Funct. Mater.* **2017**, *27*, 1702207.
[152] R. Ding, X. L. Zhang, G. Chen, H. L. Wang, R. Kishor, J. X. Xiao, F. Gao, K. Y. Zeng, X. D. Chen, X. W. Sun, Y. J. Zheng, *Nano Energy* **2017**, *37*, 126.
[153] R. Ding, H. Liu, X. L. Zhang, J. X. Xiao, R. Kishor, H. X. Sun, B. W. Zhu, G. Chen, F. Gao, X. H. Feng, J. S. Chen, X. D. Chen, X. W. Sun, Y. J. Zheng, *Adv. Funct. Mater.* **2016**, *26*, 7708.
[154] Q. F. Dong, J. F. Song, Y. J. Fang, Y. C. Shao, S. Ducharme, J. S. Huang, *Adv. Mater.* **2016**, *28*, 2816.
[155] R. Saraf, L. Pu, V. Maheshwari, A. Light Harvesting, *Adv. Mater.* **2018**, *30*, 1705778.
[156] Z. Yang, J. F. Lu, M. H. ZhuGe, Y. Cheng, J. F. Hu, F. T. Li, S. Qiao, Y. F. Zhang, G. F. Hu, Q. Yang, D. F. Peng, K. H. Liu, C. F. Pan, *Adv. Mater.* **2019**, *31*, 1900647.
[157] P. A. Franken, A. E. Hill, C. W. Peters, G. Weinreich, *Phys. Rev. Lett.* **1961**, *7*, 118.
[158] R. W. Terhune, P. D. Maker, C. M. Savage, *Phys. Rev. Lett.* **1962**, *8*, 404.
[159] J. A. Armstrong, N. Bloembergen, J. Ducuing, P. S. Pershan, *Phys. Rev.* **1962**, *127*, 1918.
[160] P. A. Franken, J. F. Ward, *Rev. Mod. Phys.* **1963**, *35*, 23.
[161] D. C. Dai, S. J. Xu, S. L. Shi, M. H. Xie, C. M. Che, *Opt. Lett.* **2005**, *30*, 3377;
[162] C. F. Zhang, F. Zhang, T. Xia, N. Kumar, J. I. Hahm, J. Liu, Z. L. Wang, J. Xu, *Opt. Express* **2009**, *17*, 7893.
[163] G. P. Zhu, C. X. Xu, J. Zhu, C. G. Lv, Y. P. Cui, *Appl. Phys. Lett.* **2009**, *94*, 051106.
[164] J. F. Lu, F. T. Li, W. D. Ma, J. F. Hu, Y. Y. Peng, Z. Yang, Q. S. Chen, C. X. Xu, C. F. Pan, Z. L. Wang, *Adv. Sci.* **2019**, *6*, 1900916.

[165] B. Crone, A. Dodabalapur, Y. Y. Lin, R. W. Filas, Z. Bao, A. LaDuca, R. Sarpeshkar, H. E. Katz, W. Li, *Nature* **2000**, *403*, 521.
[166] Q. L. Hua, J. L. Sun, H. T. Liu, R. R. Bao, R. M. Yu, J. Y. Zhai, C. F. Pan, Z. L. Wang, *Nat. Commun.* **2018**, *9*, 244.
[167] C. Dagdeviren, Y. Su, P. Joe, R. Yona, Y. H. Liu, Y. S. Kim, Y. A. Huang, A. R. Damadoran, J. Xia, L. W. Martin, Y. G. Huang, J. A. Rogers, *Nat. Commun.* **2014**, *5*, 4496.
[168] J. F. Lu, Y. Y. Peng, W. Liu, S. Qiao, F. T. Li, C. X. Kan, C. X. Xu, *J. Lumin.* **2021**, *238*, 118237.

Junfeng Lu received his B.S. degree (2010) and M.S. degree (2013) in microelectronics and solid-state electronics from Yangzhou University, China. Then he earned his Ph.D. degree (2017) from Southeast University, China. Since then, he joined the group of Professor Zhong Lin Wang at Beijing Institute of Nanoenergy and Nanosystems as a postdoctoral fellow. He is currently an associate professor at Nanjing University of Aeronautics and Astronautics. His main research interests focus on the fields of laser regulation and optoelectronic devices.

Chunxiang Xu obtained his Ph.D. degree in condensed-mater physics from Changchun Physics Research Institute, Chinese Academy of Sciences, in 1997. Then he joined the School of Electronic Science and Engineering, and the School of Biological Science and Medical Engineering, Southeast University. He worked as a research fellow at Nanyang Technology University from 2003 to 2005. His current research interests focus on optoelectronic functional nanomaterials and Biological sensing technology.

Caofeng Pan received his B.S. degree (2005) and his Ph.D. (2010) in Materials Science and Engineering from Tsinghua University, China. He then joined in the group of Professor Zhong Lin Wang at the Georgia Institute of Technology as a postdoctoral fellow. He is currently a professor and a group leader at the Beijing Institute of Nanoenergy and Nanosystems, Chinese Academy of Sciences since 2013. His main research interests focus on the fields of piezotronics/piezo-phototronics for fabricating new electronic and optoelectronic devices and self-powered nanosystems. Details can be found at http://www.piezotronics.cn/.